Syrbactin Structural Analog TIR-199 Blocks Proteasome Activity And Induces Tumor Cell Death

André S. Bachmann,[1,2,3,*] John Opoku-Ansah,[2] Tannya R. Ibarra-Rivera,[4,6] Lisette P. Yco,[1,2,3] Sudhakar Ambadi,[4] Christopher C. Roberts,[4] Chia-en A. Chang,[4] and Michael C. Pirrung[4,5*]

[1]From Department of Pediatrics and Human Development, College of Human Medicine, Michigan State University, Grand Rapids, MI 49503, USA.

[2]Department of Pharmaceutical Sciences, The Daniel K. Inouye College of Pharmacy, University of Hawaii at Hilo, Hilo, HI 96720, USA.

[3]Department of Molecular Biosciences and Bioengineering, College of Tropical Agriculture and Human Resources, University of Hawaii at Manoa, Honolulu, Hawaii 96822, USA

[4]Department of Chemistry, University of California, Riverside, CA 92521, USA.

[5]Department of Pharmaceutical Sciences, University of California, Irvine, CA 92697, USA.

[6]Current address: Department of Analytical Chemistry, Autonomous University of Nuevo León, Monterrey, Mexico

*To whom correspondence should be addressed: André S. Bachmann, Department of Pediatrics and Human Development, College of Human Medicine, Michigan State University, 301 Michigan Street, NE, Grand Rapids, MI 49503, USA. Tel.: (616) 331-5982. Fax: (616) 331-5869. E-mail: andre.bachmann@hc.msu.edu and Michael C. Pirrung, Department of Chemistry, University of California, Riverside, CA 92521, USA. Tel.: (951) 827-2722. Fax: (951) 827-2749. E-mail: Michael.pirrung@ucr.edu.

Keywords: Multiple myeloma; neuroblastoma; proteasome; natural product; computer modeling; chemical synthesis; syringolin A; TIR-199; anti-tumor activity; hollow fiber assays

ABSTRACT

Multiple myeloma (MM) is an aggressive hematopoietic cancer of plasma cells. The recent emergence of three effective FDA-approved proteasome-inhibiting drugs, bortezomib (Velcade®), carfilzomib (Kyprolis®), and ixazomib (Ninlaro®) confirms that proteasome inhibitors are therapeutically useful against neoplastic disease, in particular refractory MM and mantle cell lymphoma. This study describes the synthesis, computational affinity assessment, and preclinical evaluation of TIR-199, a natural product-derived syrbactin structural analog. Molecular modeling and simulation suggested TIR-199 covalently binds each of the three catalytic subunits (β1, β2, and β5) and revealed key interaction sites. *In vitro* and cell culture-based proteasome activity measurements confirmed that TIR-199 inhibits the proteasome in a dose-dependent manner and induces tumor cell death in multiple myeloma and neuroblastoma cells as well as other cancer types in the NCI-60 cell panel. It is particularly effective against kidney tumor cell lines, with

more than 250-fold higher anti-tumor activities than observed with the natural product syringolin A (SylA). *In vivo* studies in mice revealed a maximum tolerated dose (MTD) of TIR-199 at 25 mg/kg. The anti-tumor activity of TIR-199 was confirmed in hollow fiber assays in mice. Adverse drug reaction screens in a kidney panel revealed no off-targets of concern. This is the first study to examine the efficacy of a syrbactin in animals. Taken together, the results suggest that TIR-199 is a potent new proteasome inhibitor with promise for further development into a clinical drug for the treatment of multiple myeloma and other forms of cancer.

INTRODUCTION

Multiple Myeloma (MM) is an aggressive hematopoietic cancer of plasma cells that develops in about 6 per 100,000 people per year. MM is considered to be treatable but incurable, with a five year survival rate of 45%. After non-Hodgkin lymphoma, MM is the second most common hematological malignancy in the U.S. and constitutes 1% of all cancers (1). The current therapeutic options include six major drug classes: classic drugs like chemotherapeutic agents, corticosteroids, interferon and immunomodulatory drugs (*e.g.*, thalidomide), and more recently also proteasome inhibitors, histone deacetylase inhibitors (*e.g.*, panobinostat), and the first FDA-approved monoclonal antibody against MM, daratumumab (Darzalex®).

The recent FDA approval of the three proteasome inhibitors bortezomib (Velcade®), carfilzomib (Kyprolis®), and ixazomib (Ninlaro®) shows that the proteasome is a valuable therapeutic target against neoplastic disease (2,3). Notably, it has been shown that actively dividing cancer cells are more sensitive to proteasome inhibition than quiescent or differentiated normal cells. For example, MM cells are significantly more sensitive to the pro-apoptotic effects of bortezomib (BTZ)-induced proteasome inhibition than are healthy bone marrow cells or peripheral blood mononuclear cells (4). The differential sensitivity of cells to proteasome inhibition may in part be due to the fact that cancer cells require a higher rate of protein turnover than normal cells and, therefore, may be more susceptible to losing proteasome function. Proteasome inhibition also enhances the sensitivity of cancer cells to traditional chemotherapies, providing a rationale for the development of combination therapies.

Despite the fact that proteasome inhibition is a validated strategy for therapy of MM (5-7) and mantle cell lymphoma (8,9), this disease remains challenging as relapses are common and usually associated with increasing chemoresistance (10). Moreover, proteasome inhibitors like BTZ can induce peripheral neuropathy and other toxicities that may decrease efficacy by compromising the ability to deliver therapy at optimal doses. Thus, there are a number of shortcomings and there is an urgent need to develop next generation proteasome inhibitors with improved safety profiles for therapeutic use.

We have discovered and developed a novel class of proteasome inhibitors referred to as syrbactins (11,12). Our previous findings indicated that the natural product syringolin A (SylA) inhibits the proteasome (12-15) and induces cell death in a number of tumor cell types including MM and neuroblastoma (NB) cells (11,12,14). SylA reacts irreversibly with the *N*-terminal threonine (Thr) of the active site in the β-5 pocket by a 1,4-addition of the hydroxyl group of the Thr to the α,β-unsaturated carboxamide moiety of SylA (12). SylA preferentially inhibits the proteasomal β-5 subunit (chymotrypsin-like; CT-L) activity with a *K*i value of 0.843 μM, weakly inhibits the β2- (trypsin-like; T-L) subunit activity with a *K*i value of 6.7 μM, and has no effects on the β1- (caspase-like; C-L) subunit activity (12,15).

We previously synthesized and evaluated a number of SylA-analogs (13-22) and three other groups have designed syringolin variants (23-26). In this study, we synthesized TIR-199, one of the most potent SylA-derived compounds to date. We

demonstrate that TIR-199 inhibits the proteasome activity and impedes MM and other tumor cell growth, with a significantly higher potency than the natural product SylA, both *in vitro* and *in vivo*. Importantly, this represents the first study to examine the efficacy of a syrbactin in animals.

EXPERIMENTAL PROCEDURES

Total synthesis of Syrbactin Structural Analog TIR-199 and Reagents - The synthetic route to TIR-199 (MW 534) is provided in Scheme 1 and described in detail in the Supplemental Methods. Most of the route follows our reported syringolin A synthesis (22), with the exception of the use of alaninol. From a (*S*)-vinylglycine starting material, the route entails 10 steps and proceeds in 10% overall yield. Stocks were prepared in DMSO (10 mM). The natural product syringolin (SylA) and bortezomib (BTZ) served as controls throughout the study and were dissolved in sterile water and DMSO, respectively.

Computational Assessment of Selectivity - We used computational modeling and energetic analysis of the covalently bound complexes of TIR-199 to each proteasome receptor to understand the selectivity of TIR-199 to the catalytic receptor subtypes of the human proteasome. Because no experimental structure is available for the human proteasome, we performed homology modeling to derive the human proteasome atomic structure from the X-ray crystallographic data of the *Bos taurus* proteasome (PDB id: 1IRU), which has a sequence similarity of 99.6% to that of *Homo sapiens*. Molecular recognition takes place within a distinct binding pocket at each catalytic site in the proteasome, which includes the active catalytic enzyme and the domain directly adjacent to the active site (Fig. 2*A*). Therefore, three binding pocket structures were constructed from the homology model for use in all subsequent calculations, simulations, and analyses: The C-L (catalytic β1 and neighboring β2), T-L (catalytic β2 and neighboring β3), and CT-L (catalytic β5 and neighboring β6) binding pockets. AutoDock 4.2 was used to determine low-energy conformational states of TIR-199 within each of the catalytic receptors when bound covalently to the catalytic Thr1 active site (27). AMBER version 11 was subsequently used to perform molecular dynamics simulations starting with the bound-state conformations obtained from docking (28). The AMBER GAFF parameters were applied to the novel ligand TIR-199, while the AMBER 99SB protein forcefield parameterized the protein structures. Covalent bonds were manually formed using the AMBER xleap utility, and parameters bridging the GAFF and 99SB systems were derived from the GAFF forcefield (29). Implicit solvent Langevin dynamics simulated all systems. Ten thousand equilibration steps were performed at 100K, 200K, and 298K. Production simulations of each system were performed for 10 nanoseconds simulation time at 298K on the XSEDE national super computer system. For all simulations, a selection of protein atoms within 10Å of the ligand's initial positions defined the unconstrained, mobile region of the simulation, while the rest of the protein structure was held fixed. Trajectories of the molecular dynamics simulations were subject to molecular mechanics/generalized Born/surface area (MMGBSA) energetic post-simulation analysis to calculate accurate ligand-receptor affinities over each recorded snapshot along the simulation trajectories (30,31). The total MMGBSA interaction energy was calculated for every frame in each trajectory. The energies were separated into polar interactions, combining Coulombic and generalized Born interaction energies, and non-polar interactions, combining van der Waals and non-polar solvation solvent-accessible surface area (SASA) interaction energies.

In Vitro Proteasome Activity Assay - To determine the anti-proteasome activity of TIR-199 in the *in vitro* environment, we measured the three catalytic activities (β1, β2, β5) as previously described (12,13,15). This assay uses purified 20*S* constitutive proteasome from

human erythrocytes or immunoproteasome from human peripheral blood mononuclear cells (PBMCs) (Enzo Life Sciences) and luminogenic substrates (Z-LRR- Glo™, Z-nLPnLD-Glo™, and Suc-LLVY-Glo™), specific for the three β1, β2, and β5 catalytic subunit activities (also referred to T-L, C-L, and CT-L activities, respectively). The 20*S* proteasome and the specific luminogenic substrates were incubated individually with compounds at increasing concentrations (0 to 10 μM). Controls included the natural product SylA (20 μM) and BTZ (0.01 μM). Following cleavage by the 20*S* proteasome, the substrate for luciferase (aminoluciferin) is released, allowing the luciferase reaction to produce light. The luminescence was recorded as relative light unites (RLU) after 30 min incubation on a 96-well microplate luminometer.

In Vivo Proteasome Activity Assay - To determine the anti-proteasome activity of TIR-199 in the culture environment, the proteasome-Glo inhibition assay was performed as previously described (13,21). Solid white 96-well microtiter cell culture plates were seeded with cells and proteasome inhibition was measured using the proteasome Glo™ reagent according to the manufacturer's instructions (Promega). In brief, MM1.RL or MYCN2 cells were treated with TIR-199 at different concentrations (0-10 μM) as indicated and incubated for 2 hrs, followed by incubation for 10 min with 100 μl of proteasome Glo reagent, containing the bioluminescent substrates Suc-LLVY-aminoluciferin, Z-nLPnLD-aminoluciferin, and Z-LRR-aminoluciferin were added to measure the CT-L, C-L, and T-L activities, respectively. Luminescence was measured with a Multi-Mode Synergy™ MX Microplate Reader (BioTek, Inc.) and expressed as relative light units (RLU). SylA and BTZ were used as controls.

In Vivo Proteasome Sensor Assay - The proteasome sensor activity assay was performed in HEK-293 cells according to the manufacturer's instructions (Clontech). ZsProSensor-1 is a proteasome-sensitive fluorescent reporter, producing a fusion of green fluorescent protein (GFP) with a degradation domain (ODC) that targets the protein for rapid degradation by the proteasome. As a consequence, green fluorescence accumulates in those cells in which the proteasome is inhibited. Unlike the previous cell culture-based assay, this test does not require exogenous addition of bioluminescent substrates as it expresses an internal probe. Cells were transfected with the ZsProSensor-1 vector and tested in the presence of increasing concentrations (0-1 μM) of TIR-199 or BTZ for 24 hrs. GFP expression was quantified using an ELISA reader and pictures taken with an immunofluorescence microscope.

Mammalian Cell Cultures - The multiple myeloma (MM) cell line MM1.RL is derived from the parent cell line MM1, established from peripheral blood of a multiple myeloma patient with acquired resistance to steroid-based (dexamethasone) therapy, and was kindly provided by N. Krett (Northwestern University) (32). The human neuroblastoma (NB) cell line MYCN2 was derived from parent cell line SH-EP, and was kindly provided by Dr. J. Shohet (Texas Children's Hospital) (33). Human embryonic kidney 293 (HEK-293) cells were from the American Type Culture Collection (ATCC) (Manassas, VA, USA). HepG2 cells were tested at Cerep, Inc. (Redmond, WA, USA). Cell lines were maintained in RPMI 1640 medium (MM1.RL, MYCN2), DMEM medium (HEK-293) (Mediatech Inc., Manassas, VA, USA) or MEM alpha growth medium (HepG2). RPMI 1640 and DMEM medium contained 10 % (v/v) heat-inactivated fetal bovine serum (Invitrogen, Carlsbad, CA, USA), supplemented with penicillin (100 U/ml) and streptomycin (100 μg/ml). Cells were cultured at 37°C in a humidified atmosphere containing 5% CO_2 and seeded 16-24 hrs prior to the start of the assay.

Cell Viability Assay - The CellTiter 96® AQueous Non-Radioactive Cell Proliferation Assay is a homogeneous, colorimetric method for determining the number of viable cells in cell culture assays. The assay is composed of solutions of a novel tetrazolium compound [3-(4,5-dimethylthiazol-2-yl)-5-(3-carboxymethoxyphenyl)-2-(4-sulfophenyl)-2H-tetrazolium, inner salt; MTS] and an electron coupling reagent [phenazine methosulfate; PMS] (Promega, San Luis Obispo, CA, USA). MTS is bioreduced into soluble formazan product by dehydrogenase enzymes found in metabolically active cells. The viability of cancer cells was determined after 24 hrs treatment with TIR-199 at indicated concentrations [0-10 μM] by measuring the absorbance of the formazan product at 490 nm using a Multi-Mode Synergy™ MX Microplate Reader (BioTek, Inc., Winooski, VT, USA) as previously described (14). Data were expressed in percent (%) cell viability relative to untreated control cells. SylA and BTZ were used as positive controls.

NCI-60 Human Tumor Cell Line Screen - The NCI-60 cell line panel includes 60 human tumor cell lines. The effect of SylA and TIR-199 on tumor cell growth was tested at the National Cancer Institute, Developmental Therapeutics Program (NCI-DTP), according to their standard protocols and as previously published (34). For additional information, see: https://dtp.cancer.gov/discovery_development/nci-60/methodology.htm.

ADR Profiling - The adverse drug reaction (ADR) profile was performed at Cerep, Inc. Many ADRs are linked to off-target activities at a great variety of cellular receptors and enzymes. The effect of TIR-199 (10 μM) against the kidney organ system was tested by measuring 17 molecular targets selected on the basis of known associations of individual targets with serious ADRs as well as statistical associations derived from Cerep's proprietary BioPrint®. The following receptors/targets were individually tested: 5-HT2A, 5-HT2C, alpha2B adrenergic, beta1 adrenergic, dopamine 2S, muscarinic acetylcholine (M2, M4, M5), neurokinin 2, urotensin, and parathyroid hormone 1 receptor. In addition, activation of adenylate cyclase C and inhibition of enzymes COX2, ACE, dipeptidyl peptidase IV, phospholipase C, acetylcholinesterase was measured. The binding, activation or inhibition for each target at greater than 50% compared to control was considered a significant effect.

In Vitro Cytotoxicity Assay – This high content cytotoxicity assay was performed at Cerep, Inc. Five end points were simultaneously measured in individual cells, avoiding the drawbacks of classic *in vitro* cytotoxicity assays, which measure non-specific and late occurring cytotoxic events. The five end points are cellular parameters such as mitochondrial membrane potential (TMRM) and intracellular free calcium (Fluo-4) and more classic parameters such as nuclear size (Hoechst), membrane permeability (TOTO-3), and cell number (Hoechst), in live HepG2 cells. In brief, HepG2 cells (passage 1-15) were plated in 96-well poly D-lysine-coated plates at 3,000 cells/well in MEM alpha growth medium 16-24 hrs prior to start of the assay. One hour prior to the addition of test compound, the cells were equilibrated with assay medium containing 1% FBS. Cells were treated with TIR-199 (100 nM) or BTZ (5 nM) for 72 hrs. At the end of the incubation period, the cells were loaded for one hour with a dye cocktail containing Hoechst, TMRM, Fluo-4, and TOTO-3. Plates were scanned with an automated fluorescent microscope. Image analysis software was used to quantitate surface area (nuclear size) and fluorescence intensity (rest of end points) in defined cellular areas. Data were normalized and expressed as % of effect relative to the untreated controls. Data were also normalized using a reference compound (cerivastatin), whose maximum effect at any concentration was considered the 100% effect.

In Vivo Acute Toxicity Study - The maximum tolerated dose (MTD) study was performed at the NCI-DTP. To investigate acute toxicity of TIR-199 *in vivo*, the MTD was determined in female athymic nude mice. TIR-

199 was given by intraperitoneal (IP) injection QD x 1 on Day 0, at 12.5, 25.0, and 50.0 mg/kg/dose (groups 1-3; n=1/group). Injection volume was 0.05, 0.1 or 0.2 ml/10 gm body weight (2.5 mg/ml, homogeneous smooth suspension in 10% DMSO in Saline/Tween 80). The mice were held for 14 days post-dosing to monitor for delayed toxicity (bone marrow suppression, irreversible liver/kidney and other organ damage). For additional information, see: https://dtp.cancer.gov/organization/btb/acute_toxicity.htm.

In Vivo Hollow Fiber Assay - The *in vivo* hollow fiber assay was performed at the NCI-DTP. A solid tumor efficacy mouse model based on cell growth inside biocompatible hollow fibers was used to provide quantitative indices of drug efficacy in heterogeneous tumors with minimal time and material expenditures (35). Small hollow fibers (1 mm in diameter, 2 cm long, molecular weight exclusion of 500,000 Da), made of polyvinylidene fluoride and containing cells from human tumors, were inserted underneath the skin and in the body cavity of the mouse. A standard panel of 12 tumor cell lines, including lung, breast, colon, melanoma, ovarian, and central nervous system, was used for the routine hollow fiber screening of *in vitro* actives. Each mouse received three tumor cell lines as intraperitoneal (IP) implants, and three as subcutaneous (SC) implants. A total of 24 mice were used in 8 groups (n=3/group, each group representing two dose levels with 4 experiments, 3 cell lines/experiment) and treated by IP injection with TIR-199 starting on day 3 or 4 following fiber implantation and continuing daily for four days (QD X 4). TIR-199 was administered at two doses (9.4 mg/kg/dose or 6.3 mg/kg/dose). The selected high and low doses were based on the MTD determined in the *in vivo* acute toxicity study, using the formula: High dose = [MTD x 1.5]/4 and Low dose=0.67 x high dose. The fibers were collected from the mice on the day following the fourth compound treatment and subjected to the stable endpoint MTT assay. The optical density of each sample was determined by spectrophotometry at 540 nm, and the mean of each treatment group was calculated. The percent net growth for each cell line in each treatment group is calculated and compared to the percent net growth in the vehicle treated controls. A 50% or greater reduction in percent net growth in the treated samples compared to the vehicle control samples is considered a positive result. Each positive result is given a score of 2, and all of the scores are totaled for a given compound. The maximum possible score for an agent is 96 (12 cell lines × 2 sites × 2 dose levels × 2). A compound is considered effective and of potential interest for further xenograft studies at NCI if it has a combined IP + SC score of ≥ 20. Appropriate controls were included (n=12 for blank fibers, n=24 for vehicle controls, and n=24 for positive controls using paclitaxel). For additional information, see:https://dtp.cancer.gov/organization/btb/hollow_fiber_assay.htm.

Statistical Analyses - All experiments were performed in three independent experiments ($n = 3$) unless otherwise stated. Error bars indicate the standard error of the mean (± SEM). Data were prepared using the Microsoft Excel (Redmund, WA, USA) and GraphPad Prism 6 (La Jolla, CA, USA).

RESULTS

Structure and Synthesis of TIR-199 - The need to improve both the intrinsic potency and physicochemical properties of the syringolins led us to related natural products, the glidobactins, which were discovered based on their activity against tumor cell lines (36,37). They share a 12-membered macrodilactam, but the glidobactins have a much less hydrophilic side chain, and also differ in the amino acid (valine vs. alanine) used biosynthetically to form the α,β-unsaturated amide (Fig. 1). Since that grouping is the pharmacophore of both the syringolins and glidobactins that reacts with the essential Thr1 hydroxy group of proteasome β-subunits,

we assumed that a less sterically demanding group adjacent to the unsaturated amide could enhance activity. These considerations suggested a number of structural analogs, one of which, TIR-199, proved the most interesting (Fig. 1).

The synthetic route to TIR-199 is provided in Scheme 1 and described in detail in the Supplemental Methods section. Most of the route follows our reported syringolin A synthesis (22), with the exception of the use of alaninol. From a (*S*)-vinylglycine starting material, the route entails 10 steps and proceeds in 10% overall yield.

Computational Modeling and Docking of TIR-199 Into the Proteasome - Structure-activity relationships of the dozens of natural and synthetic syrbactins were examined to assist understanding the intrinsic activity of TIR-199 against the proteasome (Fig. 2*A*). Replacement of the syringolin R^3 with a straight-chain alkane was first reported by Kaiser's group (15), and while expected to significantly improve the cell-based activity by eliminating charge, also benefitted its intrinsic potency. Regarding the change of the larger R^1 of syringolin A to a methyl group, the proteasome's catalytic Thr1 hydroxyl approaches the unsaturated lactam adjacent to this position, making a larger grouping there a significant steric impediment (Fig. 2*B*). Syringolin A is more potent than its monounsaturated natural relative syringolin B (A-B = CH_2CH_2), and conformational analysis suggests the effect of the second alkene is to introduce strain into the macrodilactam and make it more reactive with the proteasome.

The bound-state affinities for TIR-199 to each active site within the human proteasome were calculated using MM-GBSA analysis of molecular dynamics trajectories. The most favorable interaction was found between TIR-199 and CT-L receptor due to unique non-polar stabilization. With decreasing non-polar affinity, the selectivity continues with the C-L receptor, followed by T-L receptor. The average polar and non-polar potential energies are summarized in Table 1.

TIR-199 Inhibits Catalytic Subunit Activities of the Proteasome - To measure the effect of TIR-199 on the proteasome, we measured the β1 (C-L), β2 (T-L), and β5 (CT-L) catalytic subunit activities of the proteasome. *In vitro* experiments with either purified 20*S* constitutive proteasome from human erythrocytes, or 20*S* immunoproteasome from human peripheral blood mononuclear cells (PBMCs) showed that TIR-199 strongly inhibited CT-L and T-L, but not C-L activity of the proteasome, in a dose-dependent manner (Fig. 3). Bortezomib (BTZ) was used as a control and inhibited all three constitutive proteasome activities indiscriminately but interestingly, did not inhibit the immunoproteasome T-L activity. TIR-199 displayed significantly improved potencies on the constitutive proteasome CT-L activity compared to SylA (*K*i of 0.018 and 0.843 μM (12), respectively), but was less potent than BTZ (*K*i < 0.01 μM) (Fig. 3). Interestingly, TIR-199 was less effective against the immunoproteasome CT-L activity (*K*i of ~0.075 μM) (Fig. 3*B*). Table 2 compares the activity of TIR-199 against previously reported syrbactins (SylA, GlbA, and SylA-GlbA hybrid) and bortezomib (12,13,38). The activity of TIR-199 was comparable with the activity of the SylA-GlbA hybrid.

To verify the potency against the proteasome in actively growing cell cultures, we tested TIR-199 in a cell-based, *in vivo* proteasome activity assay. TIR-199 strongly inhibited the catalytic β1, β2, and β5 subunit activities in MM1.RL cells in a dose-dependent manner (Fig. 4*A*,*C*,*E*). Similar data were obtained with MYCN2 neuroblastoma (NB) cells, confirming the activity of proteasome inhibition in two distinct cancer cell types (Fig. 4*B*,*D*,*F*). Slightly higher doses of TIR-199 were required in NB cells to achieve the effects observed in MM cells. The T-L activity in NB cells was not significantly reduced.

The effect of TIR-199 on the proteasome in actively growing cells was independently confirmed with the proteasome sensor activity assay in which the blockage of proteasome function is reflected by the accumulation of an internally overexpressed substrate (rather than externally-added substrate, as shown in Fig. 4) fused to GFP. TIR-199-treated cells as well as BTZ-treated cells showed strong accumulation of GFP compared to untreated control cells (Fig. 5). This result shows that TIR-199 is able to penetrate the membrane of intact cells and inhibits the proteasome of actively dividing cells.

TIR-199 Induces Cell Death in Multiple Myeloma and Neuroblastoma Cells - To investigate if TIR-199 induces cancer cell death, we tested increasing TIR-199 concentrations against MM and NB cells. TIR-199 killed the MM cell line MM1.RL very rapidly at the lowest concentration (0.05 μM), and inhibited NB cell viability in a dose-dependent manner between 0 and 10 μM (Fig. 4*G,H*). The concentrations to induce 50% cell death (IC_{50}) were estimated at < 0.05 μM and ~ 0.1 μM for MM and NB cells, respectively. These IC_{50} values reflect a more than 250-fold increase in potency compared to SylA that has an IC_{50} of 20-25 μM (11) and up to 39 μM in MM1.RL cells (14). The fact that TIR-199 is able to induce strong cell death in the MM1.RL cell line is particularly important and confirms that proteasome inhibition is a successful strategy to treat dexamethasone-resistant MM tumors. Table 3 compares the effect of TIR-199 on cancer cell death against previously reported syrbactins (SylA, GlbA, and SylA-GlbA hybrid) and bortezomib (11,13,14). The activity of TIR-199 was better or comparable to GlbA and SylA-GlbA hybrid.

NCI-60 Human Tumor Cell Line Screen with TIR-199 - To explore its utility in other cancer cell types, TIR-199 was tested at the National Cancer Institute Development Therapeutics Program (NCI-DTP). The results confirmed that TIR-199 induces dose-dependent cell death in a wide range of tumor cell types including breast, CNS, colon, kidney, lung, ovarian, skin, and prostate cancer, and leukemia. Of note, TIR-199 was active in a panel of kidney tumor cell lines, with exceptionally high activities in four cell lines (RXF 393, TK-10, A498, and SN12C) (Fig. 6). Compared to other groups of the NCI-60 cell panel, the renal cancer panel often does not respond well in drug screens, and, therefore, the results with TIR-199 are particularly encouraging (NCI-DTP, personal communication). TIR-199 also exhibited high activity in other cell lines, including RPMI-8226 (leukemia), NCI-H522 (non-small cell lung cancer), KM12 (colon cancer), SNB-75 (CNS cancer), LOX IMVI (melanoma), OVCAR-3 (ovarian cancer), PC-3 (prostate cancer), and BT-549 (breast cancer). Overall, our data suggest that TIR-199 is a promising anticancer agent with broad application potential against various tumor groups and selective activities in certain cell lines within each tumor group. To further demonstrate the improved anti-tumor cell activity, the initial One Dose Mean Graphs of TIR-199 was compared side-by-side with SylA, clearly showing that TIR-199 has significantly higher activity potential than the natural product SylA (Fig. 7).

Preclinical In Vitro and In Vivo Evaluation of TIR-199 - Drug induced toxicity is one of the major causes of failure during drug development and the major reason for removal of approved drugs from the market. To assess the potential of TIR-199 for preclinical development, a broad range of biological screening tests were performed. Because one potential therapeutic area identified by the NCI for TIR-199 is kidney cancer (Fig. 6), we were interested in an adverse drug reaction (ADR) assessment for kidney targets. The Cerep ADR kidney panel included 17 assays, which determine the binding of TIR-199 (10 μM) to the following targets/receptors: 5-HT2A, 5-HT2C, alpha2B adrenergic, beta1 adrenergic, dopamine 2S, muscarinic acetylcholine (M2, M4, M5), neurokinin 2, urotensin, and parathyroid hormone 1 receptor. In addition,

activation of adenylate cyclase C and inhibition of enzymes COX2, ACE, dipeptidyl peptidase IV, phospholipase C, acetylcholinesterase was measured. For the radioligand binding assays to the receptors, the strongest antagonism observed was 8% at the test concentration. Functional assays of parathyroid hormone 1 receptor and adenylate cyclase activation showed no effect of TIR-199. The enzymatic activity most affected by it was dipeptidyl peptidase IV, which was inhibited 26% at the test concentration. As an effective concentration for proteasome inhibition by TIR-199 is 1000-fold lower than these test concentrations, none of these off-target effects is considered significant (data not shown).

Additional assays were performed to determine the cytotoxicity of TIR-199 in HepG2 cells. Readouts were based on five end points that are measured simultaneously in individual cells: cell number (decreased numbers indicate cell death and/or decreased proliferation), free calcium release (uncontrolled increase in cytoplasmic calcium indicates cellular toxicity), membrane permeability (disruption of the cytoplasmic membrane indicates late cellular toxicity), mitochondrial membrane potential (indicator of respiratory capacity and cellular energetics), and nuclear size (nuclear shrinkage by chromatin condensation indicates apoptotic cell death). TIR-199 (100 nM) was tested and compared in parallel with BTZ (5 nM). The results are summarized in Table 4. Other than in direct cell killing, TIR-199 and BTZ had similar effects on intracellular calcium, nuclear size, membrane permeability, and mitochondrial membrane potential.

Due to the encouraging results of the NCI-60 cell line panel, the NCI-DTP performed *in vivo* studies in mice to determine the maximum tolerated dose (MTD) and moved TIR-199 forward into *in vivo* hollow fiber assays. Non-tumored athymic nude female mice were injected (IP) with a single dose of TIR-199 at 12.5, 25, and 50 mg/kg/dose (groups 1-3; n=1/group). At 25 mg/kg treated mice were alive at day 19 while at 50 mg/kg, the mice died on day 2, suggesting an MTD for TIR-199 of 25 mg/kg (Table 5). For comparison, the classical anti-cancer drug paclitaxel (Taxol®) is highly active at 15 mg/kg and lethal at a 30 mg/kg (NCI-DTP, personal communication). Importantly, TIR-199 at 9.4 mg/kg/dose and 6.3 mg/kg/dose (total of four doses, IP) was effective in hollow fiber studies in mice using twelve tumor cell lines (hollow fibers implanted either IP or SC) and inhibited the cell proliferation to various degrees in representing tumors of the breast, CNS, colon, lung, ovary, and skin (Table 6). Most notably, TIR-199 inhibited colon, melanoma, and ovarian tumor cells. Overall, tumor cells in IP-implanted hollow fibers responded more readily to IP-administered TIR-199, with the exception of melanoma tumors, which were also significantly inhibited in SC-implanted hollow fibers. Most but not all tumor cells that were inhibited by TIR-199 in the *in vivo* hollow fiber assay were also highly responsive in the NCI-60 cell line screen (Figure 6).

DISCUSSION

Natural products continue to offer attractive lead compounds for novel anticancer therapeutics (39), with the syrbactins as just one recent example. It is notable that the FDA-approved proteasome inhibitor carfilzomib closely resembles the peptide natural product epoxomicin. Likewise, TIR-199 addresses deficits of the original lead, SylA, through reduction of hydrophilicity and enhancement of potency. Its ligand efficiency, a broadly used measure of the potential of a compound for pharmaceutical lead development (40), based on its potency at the proteasome CT-L site is 0.28, within the desirable range.

Our understanding of TIR-199 activity was enhanced through simulation of its interaction with the chemical environment of each receptor when bound to the three catalytic sites of the proteasome. This approach revealed an interaction of the TIR-199 side chain with a proteasome pocket that is absent in any previous drug-proteasome structure (41). A

unique pocket behind the binding site of the CT-L receptor led to exceptionally high non-polar affinity and conformational stability of TIR-199 in the binding site (Fig. 2*B*). In addition, a unique rotation after the peptide bond was required for the ligand to extend into the deep pocket, lowering the internal energy of the ligand by 2.5 - 3 kcal/mol relative to the other starting conformations.

In the *in vitro* experiments, TIR-199 inhibited the β2- and β5- catalytic subunit activities in a dose-dependent fashion, with highest affinity towards the β5 subunit and only minimal activity towards the β1 subunit. This is similar to what was observed with SylA (12,15). Interestingly, in the cell-based proteasome activity assay, all three activities were inhibited in a similar fashion in MM, but not in NB cells. The reason for these differences is not clear but may in part be due to cell type-specific differences and/or differences in assay conditions (*in vitro* proteasome activity assay versus a cell-based *in vivo* proteasome activity assay) and the different sources of luminogenic substrates used in each assay. TIR-199 strongly induced tumor cell death in MM and NB cells but also in a wide range of other tumor cell lines as shown in the NCI-60 cell panel screening results (Fig. 6). Importantly, four of eight cell lines in the kidney cancer panel that traditionally responds poorly to compounds tested in the NCI-DTP drug pipeline were exceptionally sensitive to TIR-199. In the hollow fiber mouse tumor model, TIR-199 was most notably active in colon, melanoma, and ovarian tumors (Table 6). Of note, several leading drugs like bortezomib, paclitaxel, romidepsin, eribulin, sipuleucel-T, and dinutuximab (Ch14.18) were initially studied at the NCI-DTP using hollow fiber assays in mice to obtain quantitative indices of *in vivo* drug efficacy.

Proteasome inhibitors might be explored for use in diseases unrelated to cancer, in which aberrant regulation of the proteasome or immunoproteasome has been observed. Such diseases include Huntington disease (42), Alzheimer's disease (43), macular degeneration (44), inflammatory bowel disease (Crohn disease, ulcerative colitis) (45,46), and rheumatoid arthritis (Sjogren's syndrome) (47). In some instances, the use of proteasome-specific inhibitors that directly target the catalytic core might useful. For example, the proteasomal CT-L activity is increased in neurosensory retina with disease progression in age-related macular degeneration (44). In Crohn disease and ulcerative colitis proteasome inhibitors may be effective in blocking the proteasome-mediated activation of the NF-KB pathway in inflammatory bowel disease patients (45,46). In other instances, inhibitors that alter the expression of immunoproteasome-specific subunits might lead to novel treatment options. For example, the immunoproteasome-specific subunits LMP2 or LMP7 are increased in Huntington disease neurodegeneration (42) and tissue-specific upregulation of LMP7 is characteristic in patients with Sjogren's syndrome (47).

In conclusion, this is the first study that tests a syrbactin-related proteasome inhibitor in animals. We demonstrate that TIR-199 has broad-range anti-tumor activity *in vivo*. Therefore, TIR-199 and novel TIR-199-derived analogs bear significant potential for further preclinical development into a clinical drug to treat MM, kidney, and other cancer forms.

Acknowledgments

This work was supported in part by funding from the Robert C. Perry Fund of the Hawaii Community Foundation (HCF 09ADVC-45411) (to A.S.B.) and internal funds from the Daniel K. Inouye College of Pharmacy (to A.S.B.). Further support was provided by the University of California Cancer Research Coordinating Committee (to M.C.P.) and postdoctoral fellowships from UC-MEXUS and

CONACYT (to T.R.I-R). Contributions via experiment.com from Francois Souchay, Yong Rok Lee, Bruce Liu, Ann Adenbaum & Alan Schramm, and Robert Patton are also appreciated. We are most thankful to the National Cancer Institute Developmental Therapeutics Program (NCI-DTP) for performing the NCI-60 human tumor cell line screen, *in vivo* acute toxicity study, and the *in vivo* hollow fiber assays with TIR-199. We thank Dr. Paul Grothaus (NCI-DTP) for his support and for insightful discussion of results. We are grateful to Nancy L. Krett (Northwestern University, Chicago, IL, USA) and Jason Shohet (Texas Children's Hospital, Houston, TX, USA) for providing multiple myeloma cell line MM1.RL and neuroblastoma cell line MYCN2, respectively. We are indebted to Dr. Dirk Geerts (Rotterdam, the Netherlands) for excellent scientific discussion and for editing the manuscript.

Conflict of interest

A.S.B. is a named inventor of a United States patent (US 8,597,904, December 3, 2013) that relates to pharmaceutical compositions for the treatment of conditions responsive to proteasome inhibition. This patent is assigned to PONO Pharma Inc. (Honolulu, HI) for which A.S.B. currently serves as an independent agent. M.C.P is a named inventor on a United States patent application (US 2015-0141392 A1) assigned to the University of California concerning synthetic macrocyclic compounds having proteasome inhibitory activity.

Author Contributions

J.O-A. carried out all proteasome activity and cell viability experiments. T.R.I-R. and S.A. synthesized TIR-199. C.C.R. and C.A.C. made the structural models. The company Cerep, Inc. performed the ADR profiling and HepG2 *in vitro* cytotoxicity studies. L.P.Y. performed the statistical analyses of proteasome and cell viability assays. The NCI-DTP screened the NCI-60 cell panel and performed the *in vivo* MTD and hollow fiber studies. A.S.B. and M.C.P. designed the study. A.S.B., M.C.P., C.A.C, and C.C.R. wrote the paper with comments from all other authors.

References

1. Raab, M. S., Podar, K., Breitkreutz, I., Richardson, P. G., and Anderson, K. C. (2009) Multiple myeloma. *Lancet* **374**, 324-339
2. Bross, P. F., Kane, R., Farrell, A. T., Abraham, S., Benson, K., Brower, M. E., Bradley, S., Gobburu, J. V., Goheer, A., Lee, S. L., Leighton, J., Liang, C. Y., Lostritto, R. T., McGuinn, W. D., Morse, D. E., Rahman, A., Rosario, L. A., Verbois, S. L., Williams, G., Wang, Y. C., and Pazdur, R. (2004) Approval summary for bortezomib for injection in the treatment of multiple myeloma. *Clin Cancer Res* **10**, 3954-3964
3. Herndon, T. M., Deisseroth, A., Kaminskas, E., Kane, R. C., Koti, K. M., Rothmann, M. D., Habtemariam, B., Bullock, J., Bray, J. D., Hawes, J., Palmby, T. R., Jee, J., Adams, W., Mahayni, H., Brown, J., Dorantes, A., Sridhara, R., Farrell, A. T., and Pazdur, R. (2013) U.s. Food and Drug Administration approval: carfilzomib for the treatment of multiple myeloma. *Clin Cancer Res* **19**, 4559-4563
4. Adams, J. (2004) The proteasome: a suitable antineoplastic target. *Nat Rev Cancer* **4**, 349-360
5. Richardson, P. G., Barlogie, B., Berenson, J., Singhal, S., Jagannath, S., Irwin, D., Rajkumar, S. V., Srkalovic, G., Alsina, M., Alexanian, R., Siegel, D., Orlowski, R. Z., Kuter, D., Limentani, S.

A., Lee, S., Hideshima, T., Esseltine, D. L., Kauffman, M., Adams, J., Schenkein, D. P., and Anderson, K. C. (2003) A phase 2 study of bortezomib in relapsed, refractory myeloma. *N Engl J Med* **348**, 2609-2617

6. Richardson, P. G., Sonneveld, P., Schuster, M., Irwin, D., Stadtmauer, E., Facon, T., Harousseau, J. L., Ben-Yehuda, D., Lonial, S., Goldschmidt, H., Reece, D., Miguel, J. S., Blade, J., Boccadoro, M., Cavenagh, J., Alsina, M., Rajkumar, S. V., Lacy, M., Jakubowiak, A., Dalton, W., Boral, A., Esseltine, D. L., Schenkein, D., and Anderson, K. C. (2007) Extended follow-up of a phase 3 trial in relapsed multiple myeloma: final time-to-event results of the APEX trial. *Blood* **110**, 3557-3560
7. Richardson, P. G., Sonneveld, P., Schuster, M. W., Irwin, D., Stadtmauer, E. A., Facon, T., Harousseau, J. L., Ben-Yehuda, D., Lonial, S., Goldschmidt, H., Reece, D., San-Miguel, J. F., Blade, J., Boccadoro, M., Cavenagh, J., Dalton, W. S., Boral, A. L., Esseltine, D. L., Porter, J. B., Schenkein, D., Anderson, K. C., and Assessment of Proteasome Inhibition for Extending Remissions, I. (2005) Bortezomib or high-dose dexamethasone for relapsed multiple myeloma. *N Engl J Med* **352**, 2487-2498
8. Fisher, R. I., Bernstein, S. H., Kahl, B. S., Djulbegovic, B., Robertson, M. J., de Vos, S., Epner, E., Krishnan, A., Leonard, J. P., Lonial, S., Stadtmauer, E. A., O'Connor, O. A., Shi, H., Boral, A. L., and Goy, A. (2006) Multicenter phase II study of bortezomib in patients with relapsed or refractory mantle cell lymphoma. *J Clin Oncol* **24**, 4867-4874.
9. Strauss, S. J., Maharaj, L., Hoare, S., Johnson, P. W., Radford, J. A., Vinnecombe, S., Millard, L., Rohatiner, A., Boral, A., Trehu, E., Schenkein, D., Balkwill, F., Joel, S. P., and Lister, T. A. (2006) Bortezomib therapy in patients with relapsed or refractory lymphoma: potential correlation of in vitro sensitivity and tumor necrosis factor alpha response with clinical activity. *J Clin Oncol* **24**, 2105-2112.
10. Lu, S., and Wang, J. (2013) The resistance mechanisms of proteasome inhibitor bortezomib. *Biomark Res* **1**, 13
11. Coleman, C. S., Rocetes, J. P., Park, D. J., Wallick, C. J., Warn-Cramer, B. J., Michel, K., Dudler, R., and Bachmann, A. S. (2006) Syringolin A, a new plant elicitor from the phytopathogenic bacterium Pseudomonas syringae pv. syringae, inhibits the proliferation of neuroblastoma and ovarian cancer cells and induces apoptosis. *Cell Prolif* **39**, 599-609.
12. Groll, M., Schellenberg, B., Bachmann, A. S., Archer, C. R., Huber, R., Powell, T. K., Lindow, S., Kaiser, M., and Dudler, R. (2008) A plant pathogen virulence factor inhibits the eukaryotic proteasome by a novel mechanism. *Nature* **452**, 755-758
13. Archer, C. R., Groll, M., Stein, M. L., Schellenberg, B., Clerc, J., Kaiser, M., Kondratyuk, T. P., Pezzuto, J. M., Dudler, R., and Bachmann, A. S. (2012) Activity enhancement of the synthetic syrbactin proteasome inhibitor hybrid and biological evaluation in tumor cells. *Biochemistry* **51**, 6880-6888
14. Archer, C. R., Koomoa, D. L., Mitsunaga, E. M., Clerc, J., Shimizu, M., Kaiser, M., Schellenberg, B., Dudler, R., and Bachmann, A. S. (2010) Syrbactin class proteasome inhibitor-induced apoptosis and autophagy occurs in association with p53 accumulation and Akt/PKB activation in neuroblastoma. *Biochem Pharmacol* **80**, 170-178
15. Clerc, J., Groll, M., Illich, D. J., Bachmann, A. S., Huber, R., Schellenberg, B., Dudler, R., and Kaiser, M. (2009) Synthetic and structural studies on syringolin A and B reveal critical determinants of selectivity and potency of proteasome inhibition. *Proc Natl Acad Sci U S A* **106**, 6507-6512

16. Anshu, A., Thomas, S., Agarwal, P., Ibarra-Rivera, T. R., Pirrung, M. C., and Schonthal, A. H. (2011) Novel proteasome-inhibitory syrbactin analogs inducing endoplasmic reticulum stress and apoptosis in hematological tumor cell lines. *Biochem Pharmacol* **82**, 600-609
17. Clerc, J., Florea, B. I., Kraus, M., Groll, M., Huber, R., Bachmann, A. S., Dudler, R., Driessen, C., Overkleeft, H. S., and Kaiser, M. (2009) Syringolin A selectively labels the 20 S proteasome in murine EL4 and wild-type and bortezomib-adapted leukaemic cell lines. *Chembiochem* **10**, 2638-2643
18. Clerc, J., Li, N., Krahn, D., Groll, M., Bachmann, A. S., Florea, B. I., Overkleeft, H. S., and Kaiser, M. (2011) The natural product hybrid of Syringolin A and Glidobactin A synergizes proteasome inhibition potency with subsite selectivity. *Chem Commun (Camb)* **47**, 385-387
19. Clerc, J., Schellenberg, B., Groll, M., Bachmann, A. S., Huber, R., Dudler, R., and Kaiser, M. (2010) Convergent synthesis and biological evaluation of Syringolin A and derivatives as eukaryotic 20S proteasome inhibitors. *Eur J Org Chem* **21**, 3991-4003
20. Ibarra-Rivera, T. R., Opoku-Ansah, J., Ambadi, S., Bachmann, A. S., and Pirrung, M. C. (2011) Syntheses and cytotoxicity of syringolin B-based proteasome inhibitors. *Tetrahedron* **67**, 9950-9956
21. Opoku-Ansah, J., Ibarra-Rivera, T. R., Pirrung, M. C., and Bachmann, A. S. (2012) Syringolin B-inspired proteasome inhibitor analogue TIR-203 exhibits enhanced biological activity in multiple myeloma and neuroblastoma. *Pharm Biol* **50**, 25-29
22. Pirrung, M. C., Biswas, G., and Ibarra-Rivera, T. R. (2010) Total synthesis of syringolin A and B. *Org Lett* **12**, 2402-2405
23. Chiba, T., Hosono, H., Nakagawa, K., Asaka, M., Takeda, H., Matsuda, A., and Ichikawa, S. (2014) Total synthesis of syringolin A and improvement of its biological activity. *Angew Chem Int Ed Engl* **53**, 4836-4839
24. Chiba, T., Matsuda, A., and Ichikawa, S. (2015) Structure-activity relationship study of syringolin A as a potential anticancer agent. *Bioorg Med Chem Lett* **25**, 4872-4877.
25. Totaro, K. A., Barthelme, D., Simpson, P. T., Sauer, R. T., and Sello, J. K. (2015) Substrate-guided optimization of the syringolins yields potent proteasome inhibitors with activity against leukemia cell lines. *Bioorg Med Chem* **23**, 6218-6222
26. Trivella, D. B., Pereira, A. R., Stein, M. L., Kasai, Y., Byrum, T., Valeriote, F. A., Tantillo, D. J., Groll, M., Gerwick, W. H., and Moore, B. S. (2014) Enzyme inhibition by hydroamination: design and mechanism of a hybrid carmaphycin-syringolin enone proteasome inhibitor. *Chem Biol* **21**, 782-791
27. Morris, G. M., Huey, R., Lindstrom, W., Sanner, M. F., Belew, R. K., Goodsell, D. S., and Olson, A. J. (2009) AutoDock4 and AutoDockTools4: Automated docking with selective receptor flexibility. *J Comput Chem* **30**, 2785-2791
28. Case, D. A., Cheatham, T. E., 3rd, Darden, T., Gohlke, H., Luo, R., Merz, K. M., Jr., Onufriev, A., Simmerling, C., Wang, B., and Woods, R. J. (2005) The Amber biomolecular simulation programs. *J Comput Chem* **26**, 1668-1688
29. Wang, J., Wolf, R. M., Caldwell, J. W., Kollman, P. A., and Case, D. A. (2004) Development and testing of a general amber force field. *J Comput Chem* **25**, 1157-1174
30. Massova, I., and Kollman, P. A. (2000) Combined molecular mechanical and continuum solvent approach (MM-PBSA/GBSA) to predict ligand binding. *Perspect Drug Discov Des* **18**, 113-135
31. Tsui, V., and Case, D. A. (2000) Theory and applications of the generalized Born solvation model in macromolecular simulations. *Biopolymers* **56**, 275-291

32. Greenstein, S., Krett, N. L., Kurosawa, Y., Ma, C., Chauhan, D., Hideshima, T., Anderson, K. C., and Rosen, S. T. (2003) Characterization of the MM.1 human multiple myeloma (MM) cell lines: a model system to elucidate the characteristics, behavior, and signaling of steroid-sensitive and -resistant MM cells. *Exp Hematol* **31**, 271-282
33. Slack, A., Chen, Z., Tonelli, R., Pule, M., Hunt, L., Pession, A., and Shohet, J. M. (2005) The p53 regulatory gene MDM2 is a direct transcriptional target of MYCN in neuroblastoma. *Proc Natl Acad Sci U S A* **102**, 731-736
34. Shoemaker, R. H. (2006) The NCI60 human tumour cell line anticancer drug screen. *Nat Rev Cancer* **6**, 813-823
35. Hollingshead, M. G., Alley, M. C., Camalier, R. F., Abbott, B. J., Mayo, J. G., Malspeis, L., and Grever, M. R. (1995) In vivo cultivation of tumor cells in hollow fibers. *Life Sci* **57**, 131-141
36. Oka, M., Nishiyama, Y., Ohta, S., Kamei, H., Konishi, M., Miyaki, T., Oki, T., and Kawaguchi, H. (1988) Glidobactins A, B and C, new antitumor antibiotics. I. Production, isolation, chemical properties and biological activity. *J Antibiot (Tokyo)* **41**, 1331-1337
37. Oka, M., Numata, K., Nishiyama, Y., Kamei, H., Konishi, M., Oki, T., and Kawaguchi, H. (1988) Chemical modification of the antitumor antibiotic glidobactin. *J Antibiot (Tokyo)* **41**, 1812-1822
38. Adams, J., Behnke, M., Chen, S., Cruickshank, A. A., Dick, L. R., Grenier, L., Klunder, J. M., Ma, Y. T., Plamondon, L., and Stein, R. L. (1998) Potent and selective inhibitors of the proteasome: dipeptidyl boronic acids. *Bioorg Med Chem Lett* **8**, 333-338
39. Cragg, G. M., Grothaus, P. G., and Newman, D. J. (2009) Impact of natural products on developing new anti-cancer agents. *Chem Rev* **109**, 3012-3043
40. Hopkins, A. L., Keseru, G. M., Leeson, P. D., Rees, D. C., and Reynolds, C. H. (2014) The role of ligand efficiency metrics in drug discovery. *Nat Rev Drug Discov* **13**, 105-121
41. Borissenko, L., and Groll, M. (2007) 20S proteasome and its inhibitors: crystallographic knowledge for drug development. *Chem Rev* **107**, 687-717.
42. Diaz-Hernandez, M., Hernandez, F., Martin-Aparicio, E., Gomez-Ramos, P., Moran, M. A., Castano, J. G., Ferrer, I., Avila, J., and Lucas, J. J. (2003) Neuronal induction of the immunoproteasome in Huntington's disease. *J Neurosci* **23**, 11653-11661
43. Mishto, M., Bellavista, E., Santoro, A., Stolzing, A., Ligorio, C., Nacmias, B., Spazzafumo, L., Chiappelli, M., Licastro, F., Sorbi, S., Pession, A., Ohm, T., Grune, T., and Franceschi, C. (2006) Immunoproteasome and LMP2 polymorphism in aged and Alzheimer's disease brains. *Neurobiol Aging* **27**, 54-66
44. Ethen, C. M., Hussong, S. A., Reilly, C., Feng, X., Olsen, T. W., and Ferrington, D. A. (2007) Transformation of the proteasome with age-related macular degeneration. *FEBS Lett* **581**, 885-890
45. Fitzpatrick, L. R., Small, J. S., Poritz, L. S., McKenna, K. J., and Koltun, W. A. (2007) Enhanced intestinal expression of the proteasome subunit low molecular mass polypeptide 2 in patients with inflammatory bowel disease. *Dis Colon Rectum* **50**, 337-348; discussion 348-350
46. Visekruna, A., Joeris, T., Seidel, D., Kroesen, A., Loddenkemper, C., Zeitz, M., Kaufmann, S. H., Schmidt-Ullrich, R., and Steinhoff, U. (2006) Proteasome-mediated degradation of IkappaBalpha and processing of p105 in Crohn disease and ulcerative colitis. *J Clin Invest* **116**, 3195-3203
47. Egerer, T., Martinez-Gamboa, L., Dankof, A., Stuhlmuller, B., Dorner, T., Krenn, V., Egerer, K., Rudolph, P. E., Burmester, G. R., and Feist, E. (2006) Tissue-specific up-regulation of the proteasome subunit beta5i (LMP7) in Sjogren's syndrome. *Arthritis and rheumatism* **54**, 1501-1508

FOOTNOTES

[1]From Department of Pediatrics and Human Development, College of Human Medicine, Michigan State University, Grand Rapids, MI 49503, USA.
[2]Department of Pharmaceutical Sciences, The Daniel K. Inouye College of Pharmacy, University of Hawaii at Hilo, Hilo, HI 96720, USA.
[3]Department of Molecular Biosciences and Bioengineering, College of Tropical Agriculture and Human Resources, University of Hawaii at Manoa, Honolulu, Hawaii 96822, USA
[4]Department of Chemistry, University of California, Riverside, CA 92521, USA.
[5]Department of Pharmaceutical Sciences, University of California, Irvine, CA 92697, USA.
[6]Current address: Department of Analytical Chemistry, Autonomous University of Nuevo León, Monterrey, Mexico

The abbreviations used are: BTZ, bortezomib; SylA, Syringolin A; MM, multiple myeloma; MTD, maximum tolerated dose; CT-L, chymotrypsin-like; C-L, caspase-like; T-L, trypsin-like

SCHEME 1. **Total synthesis of TIR-199**. Molecular weight (MW) of TIR-199: 534.

FIGURE 1**. The chemical structures of syringolin A (SylA), glidobactin A (GlbA), and their structural analog TIR-199.** SylA is a natural product from *Pseudomonas syringae* pv. *syringae*. GlbA is from *Polyangium brachysporum*. Together, this group of proteasome inhibitors is referred to as syrbactins. TIR-199 is one of several syrbactin-derived structural analogs with superior inhibitory activities. MW of TIR-199 is 534.

FIGURE 2. **Human proteasome catalytic β ring homology model.** *A,* Protein domains are differentiated by color. Catalytic active site Thr1 residues shown with spacefill graphical representations. *B,* TIR-199 bound to the chymotrypsin-like (CT-L) receptor of the human proteasome. A unique pocket exposed to the surface of the proteasome complex is visible behind TIR-199. Extension of the hydrophobic tail into this pocket leads to increased affinity and stability.

FIGURE 3. **TIR-199 inhibits the proteasome activity *in vitro.*** The inhibitory effect of increasing concentrations of TIR-199 (0-5 μM) on the chymotrypsin-like (CT-L), caspase-like (C-L), and trypsin-like (T-L) catalytic subunit activities of the (*A*) constitutive proteasome and (*B*) immunoproteasome were measured, using luminogenic substrates as described in the material and methods section. Bortezomib (BTZ) was used as a positive control (0.01 μM). The relative light units (RLU) for each catalytic subunit activity were expressed as "remaining activity in %", where 100% activity represents the control (untreated proteasome). Data represent the average of three independent experiments (n=3); bars, mean ± SEM.

FIGURE 4. **TIR-199 inhibits the proteasomal activity and cell viability of actively-dividing cancer cells.** TIR-199 inhibited the chymotrypsin-like (CT-L) (*A*), caspase-like (C-L) (*B*), and trypsin-like (T-L) (*C*) catalytic subunit activities of the dexamethasone-resistant multiple myeloma (MM) cell line MM1.RL (*A-D*), and the neuroblastoma (NB) cell line MYCN2 (*E-H*), respectively. Cells were treated for 2 h with TIR-199 at various concentrations (0-10 μM). SylA and bortezomib (BTZ) were used as controls. The proteasomal activities were measured as outlined in the material and methods section. TIR-199 induced rapid death of MM1.RL (*D*) and MYCN2 cells (*H*). Cells were treated over a period of 24 hrs with TIR-199 at various concentrations (0-10 μM). SylA and BTZ were used as a control. The viability of cells is expressed as percent (%) cell survival relative to untreated control cells and was determined by MTS assay as outlined in the material and methods. Data represent the average of three independent experiments (n=3); bars, mean ± SEM.

FIGURE 5. **TIR-199 inhibited the proteasome activity in human embryonic kidney cells HEK-293 cells using a proteasome sensor cell transfection assay.** *A*, HEK-293 cells transfected with the ZsProSensor-1 plasmid were treated with the indicated concentrations of TIR-199 and BTZ and quantified for GFP expression as a marker for proteasome inhibition. *B*, Fluorescent microscope images of GFP-expressing cells treated with TIR-199, BTZ or control, after 24 hrs exposure.

FIGURE 6. **Antiproliferative effect of proteasome inhibitor TIR-199 in the NCI-60 human tumor cell line panel.** Dose-response curves for TIR-199 (NSC:761526). *A,* A panel of 60 human tumor cell lines representing nine different cancerous tissues of origin (leukemia, non-small cell lung cancer, colon cancer, CNS cancer, melanoma, ovarian cancer, renal cancer, prostate cancer, and breast cancer) was tested at the National Cancer Institute Developmental Therapeutics Program (NCI-DTP) in the presence of TIR-199 at five concentrations. TIR-199 was tested over a 10,000-fold concentration range in a 2-day assay and exhibited dose-dependent growth inhibition to various degrees, in all tested tumor cell lines. *B,* Dose-response data of (*A*) were used to calculate three endpoints for each cell line – GI50 (the Log_{10} of the concentration that caused 50% growth inhibition), TGI (the Log_{10} of the concentration that caused total growth inhibition), and LC50 (the Log_{10} of the concentration that caused 50% lethality). For each endpoint the mean across all the cell lines was calculated. The GI50 data are graphed as the difference of the GI50 for a particular cell line from the mean GI50. Cell lines that are more sensitive are represented as bars deflecting to the right of the mean and less sensitive cell lines project to the left of the mean. TGI and LC50 Mean Graphs are generated in a similar fashion. One representative data set of three independent experiments is shown (n=3), except for the leukemia cell panel (n=2). For additional information about the NCI-60 cell line panel, see [34] and Experimental Procedures.

FIGURE 7. **Mean Graphs display of NCI-60 cell line screening data for TIR-199.** One Dose Mean Graph display of NCI-60 cell line screening data for (*A*) TIR-199 (NSC:761526) and (*B*) SylA (NSC:749671) at 10 μM. Bars to the right indicate high sensitivity, bars to the left indicate low sensitivity to TIR-199 (*A*) and SylA (*B*). For additional information about the NCI-60 human cancer cell line screen, see [34] and Experimental Procedures. Experiments were performed at the NCI-DTP.

Table 1

Proteasome/TIR-199 affinity	Polar	Non-polar	Total
Caspase-like (C-L)	-26.24	-36.37	-62.61
Trypsin-like (T-L)	-25.96	-32.39	-58.35
Chymotrypsin-like (CT-L)	-26.66	-41.6	-68.26

Table 1. Bound-state potential energy between TIR-199 and each receptor subtype of the human proteasome. Values are calculated for, and averaged over, each simulation snapshot of the simulation trajectories (kcal/mol).

Table 2

	Ki (nM)				
Activity	TIR-199	SylA[1]	GlbA[1]	SylA-GlbA[2]	BTZ[3]
CT-L (β5)	18	843	49	12.5	0.62
T-L (β2)	194	6,700	2,000	136.9	n.d.
C-L (β1)	>5,000*	n.d.	n.d.	3,700	n.d.

Table 2. Inhibitory effects of syrbactins on proteasome activity *in vitro*. Three proteasomal activities were measured; chymotrypsin-like, CT-L (β5); trypsin-like, T-L (β2); caspase-like, C-L (β1). *Minimal activity at the highest tested concentration (5,000 nM). SylA, Syringolin A; SylA-GlbA, Syringolin A-Glidobactin A hybrid; BTZ, Bortezomib (Velcade®); n.d., not determined. Values in this table are either derived from this study (Figure 3*A*) or are historic values from the published literature [1]*Nature*, 2008, 455: 755-758 (12); [2]*Biochemistry*, 2012, 51: 6880−6888 (13); [3]*Bioorg Med Chem Lett*, 1998, 8: 333-338 (38).

Table 3

	IC_{50} (nM)[a]				
Cell Line	TIR-199	SylA[1,2]	GlbA[2]	SylA-GlbA[3]	BTZ[2]
SK-N-SH	100*	25,000	94	321	4.8
MM1.S	n.d.	8,500	4	28	2.4
MM1.RL	<50	39,300	5	27	3.0
U266	n.d.	n.d.	548	45	3.4
SKOV-3	n.d.	20,000	852	109	39.9

Table 3. Effect of TIR-199 and other syrbactins on cancer cell death. Bortezomib was used as control for comparison. [a]IC_{50}= inhibitory concentration at which cell viability is reduced by 50%. *Instead of SK-N-SH, the MYCN2 cell line was used in experiments with TIR-199. MYCN2 represents the neuroblastoma cell line SHEP which was previoulsy transfected with a tetracycline on/off plasmid system to allow for controlled MYCN expression (33). SHEP is the S-type sub-clone of the cell line SK-N-SH. Data present the mean values of three independent experiments, each performed in duplicate wells (n=6). SylA, Syringolin A; SylA-GlbA, Syringolin A-Glidobactin A hybrid; BTZ, Bortezomib (Velcade®); n.d., not determined. Values are either derived from this study (Figure 4*G*,*H*) or are historic values from the published literature [1]*Cell Prolif*, 2006, 39: 599-609 (11); [2]*Biochem Pharmacol*, 2010, 80: 170-178 (14); [3]*Biochemistry*, 2012, 51: 6880−6888 (13).

Table 4

Test	TIR-199 (100 nM)	BTZ (5 nM)
Cell number	62%	98%
Intracellular free Ca^{++}	27%	29%
Nuclear size	84%	92%
Membrane permeability	93%	99%
Mito membrane potential	98%	100%

Table 4. Values represent % effect (% cytotoxicity) relative to untreated controls. This includes - cell number: % reduction; intracellular free calcium: % increase; nuclear size: % reduction; membrane permeability: % increase; mitochondrial membrane potential: % reduction. Data represent the mean of triplicate wells (n=3).

Table 5

Group	Dose/Units (IP)	Schedule	Death Days	Survival/Total (Day 19)
1	12.5 mg/kg/dose	QD X 1, Day 0	-	1/1
2	25.0 mg/kg/dose	QD X 1, Day 0	-	1/1
3	50.0 mg/kg/dose	QD X 1, Day 0	2	0/1

Table 5. *In vivo* acute toxicity study. The maximum tolerated dose (MTD) of TIR-199 was determined in athymic nude female mice as described under Experimental Procedures. TIR-199 was tested at three doses (IP single injection) and a MTD of 25 mg/kg was determined. Group 1-3; n=1/group. IP, intraperitoneal. Experiments were performed at the NCI-DTP.

Table 6

			% Cell Growth		
Cell Line	**HF implant (IP) 6.30 mg/kg (IP)**	**HF implant (IP) 9.40 mg/kg (IP)**	**HF implant (SC) 6.30 mg/kg (IP)**	**HF implant (SC) 9.40 mg/kg (IP)**	**Tumor Group**
COLO 205	78	25	100	60	Colon
SW-620	109	91	106	73	Colon
LOX IMVI	162	53	107	28	Skin/Melanoma
MDA-MB-435	44	24	80	48	Skin/Melanoma
UACC-62	115	88	114	106	Skin/Melanoma
MDA-MB-231	92	66	87	97	Breast
NCI-H23	85	75	101	108	Non-Small Cell Lung
NCI-522	95	49	124	96	Non-Small Cell Lung
OVCAR-3	97	45	93	65	Ovary
OVCAR-5	44	22	95	75	Ovary
SF-295	72	48	95	77	CNS
U251	97	54	115	97	CNS

Table 6. *In vivo* hollow fiber assays to assess anti-tumor efficacy of TIR-199 (NSC:761526) in mice. Twelve cancer cell lines were tested in mice, representing the following tumor groups: colon (COLO 205, SW-620), skin/melanoma (LOX IMVI, MDA-MB-435, UACC-62), breast (MDA-MB-231), non-small cell lung (NCI-H23, NCI-H522), ovary (OVCAR-3, OVCAR-5), and CNS (SF-295, U251). These 12 cell lines represent a standard panel selected by the NCI-DTP based on good tumor growth performance in the HF assay. Cell lines were implanted (IP or SC) and mice treated (IP) at 6.4 mg/kg/dose or 9.3 mg/kg/dose daily, for four days (QD X 4), as described in the Experimental Procedures. Values represent the percentage (%) of cell growth. Underlined values indicate cell lines with ≥50% growth inhibition, which is considered a positive result to determine the total score. The total score for TIR-199 was 20 (IP: 2x8 cell lines =16 and SC: 2x2 cell lines=4). IP, intraperitoneal; SC, subcutaneous; HF, hollow fiber. Experiments were performed at the NCI-DTP.

Scheme S1

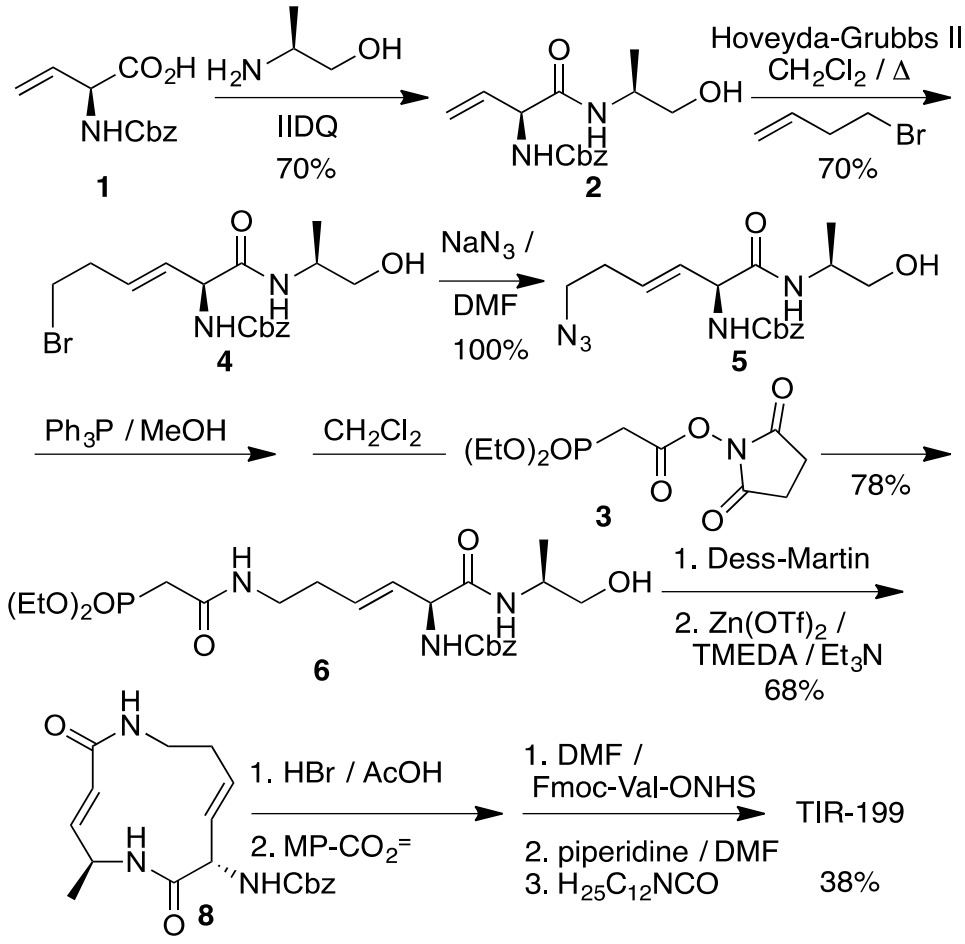
CO2H
NHCbz
1
H2N
OH
IIDQ
70%
O
N
H
OH
NHCbz
2
Hoveyda-Grubbs II
CH2Cl2 / Δ
Br
70%
Br
4
NaN3 /
DMF
100%
N3
5
Ph3P / MeOH
CH2Cl2
(EtO)2OP
O
N
O
3
78%
(EtO)2OP
6
1. Dess-Martin
2. Zn(OTf)2 /
TMEDA / Et3N
68%
1. HBr / AcOH
2. MP-CO2=
1. DMF /
Fmoc-Val-ONHS
2. piperidine / DMF
3. H25C12NCO
TIR-199
38%
8

Figure 1

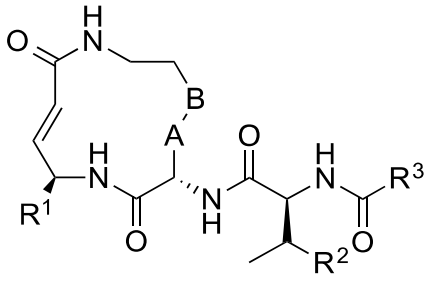

	A–B	R^1	R^2	R^3
syringolin A	HC=CH	*i*Pr	Me	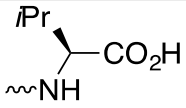
glidobactin A	H_2C–CHOH	Me	OH	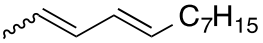
TIR-199	HC=CH	Me	Me	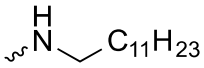

Figure 2

A

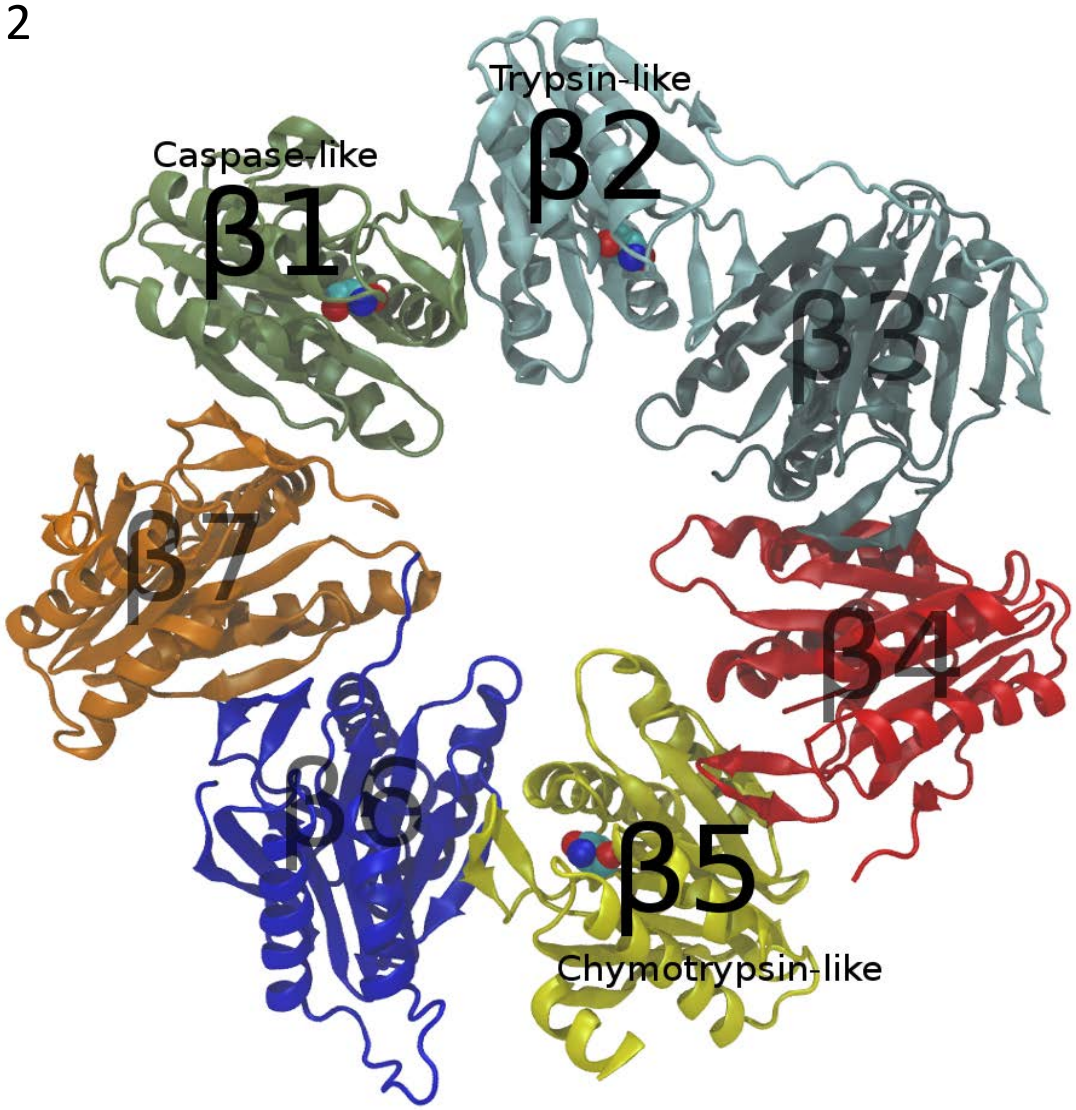
Trypsin-like
β2
Caspase-like
β1
β3
β7
β4
β6
β5
Chymotrypsin-like

B

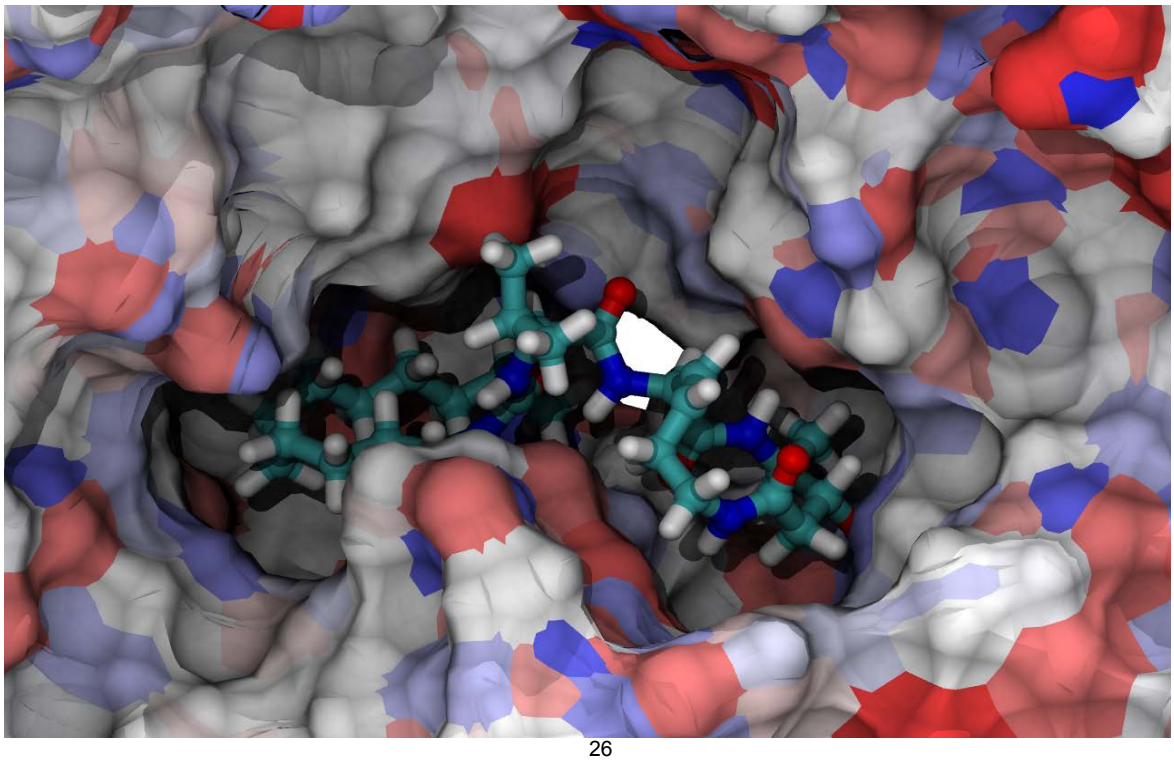

Figure 3

A

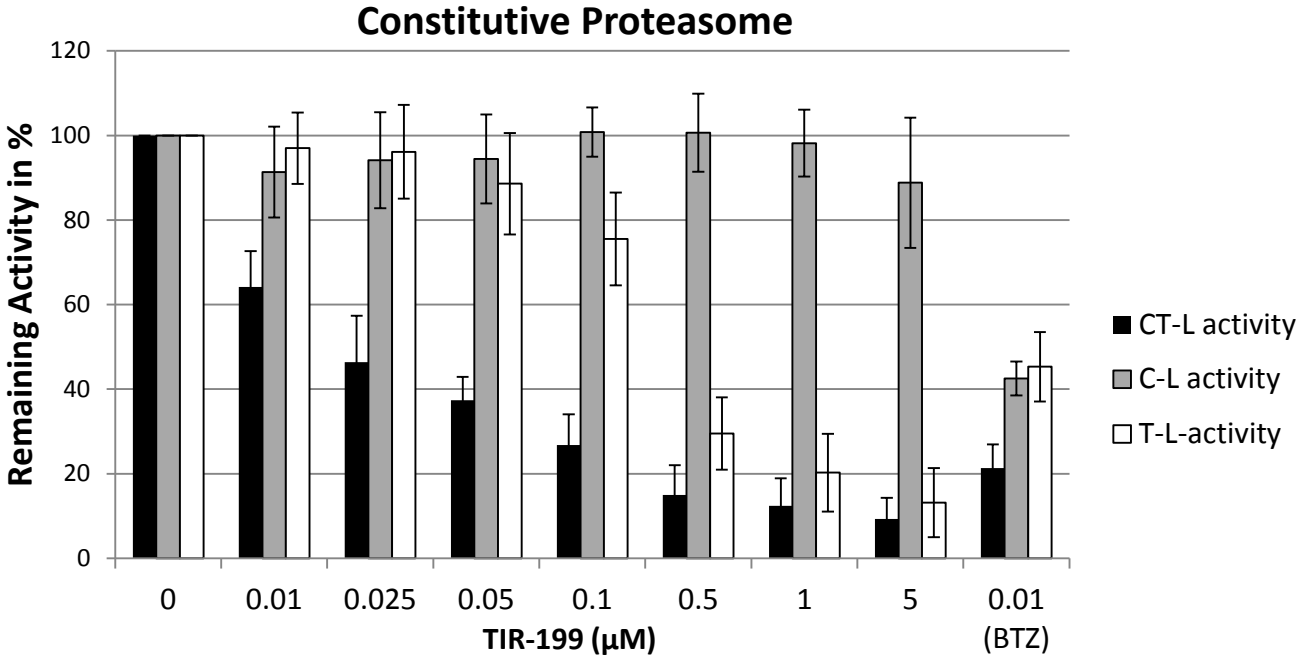
Constitutive Proteasome
Remaining Activity in %
120
100
80
60
40
20
0
0
0.01
0.025
0.05
0.1
0.5
1
5
0.01
(BTZ)
TIR-199 (µM)
CT-L activity
C-L activity
T-L-activity

B

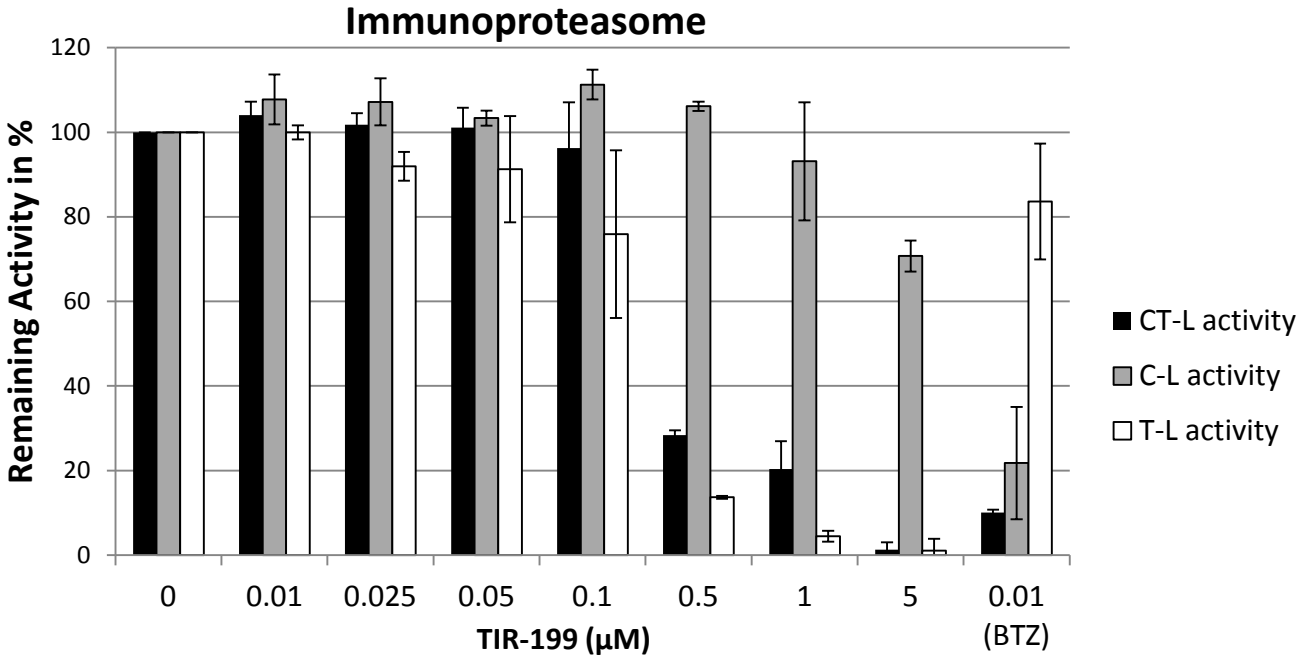
Immunoproteasome
Remaining Activity in %
120
100
80
60
40
20
0
0
0.01
0.025
0.05
0.1
0.5
1
5
0.01
(BTZ)
TIR-199 (µM)
CT-L activity
C-L activity
T-L activity

Figure 4

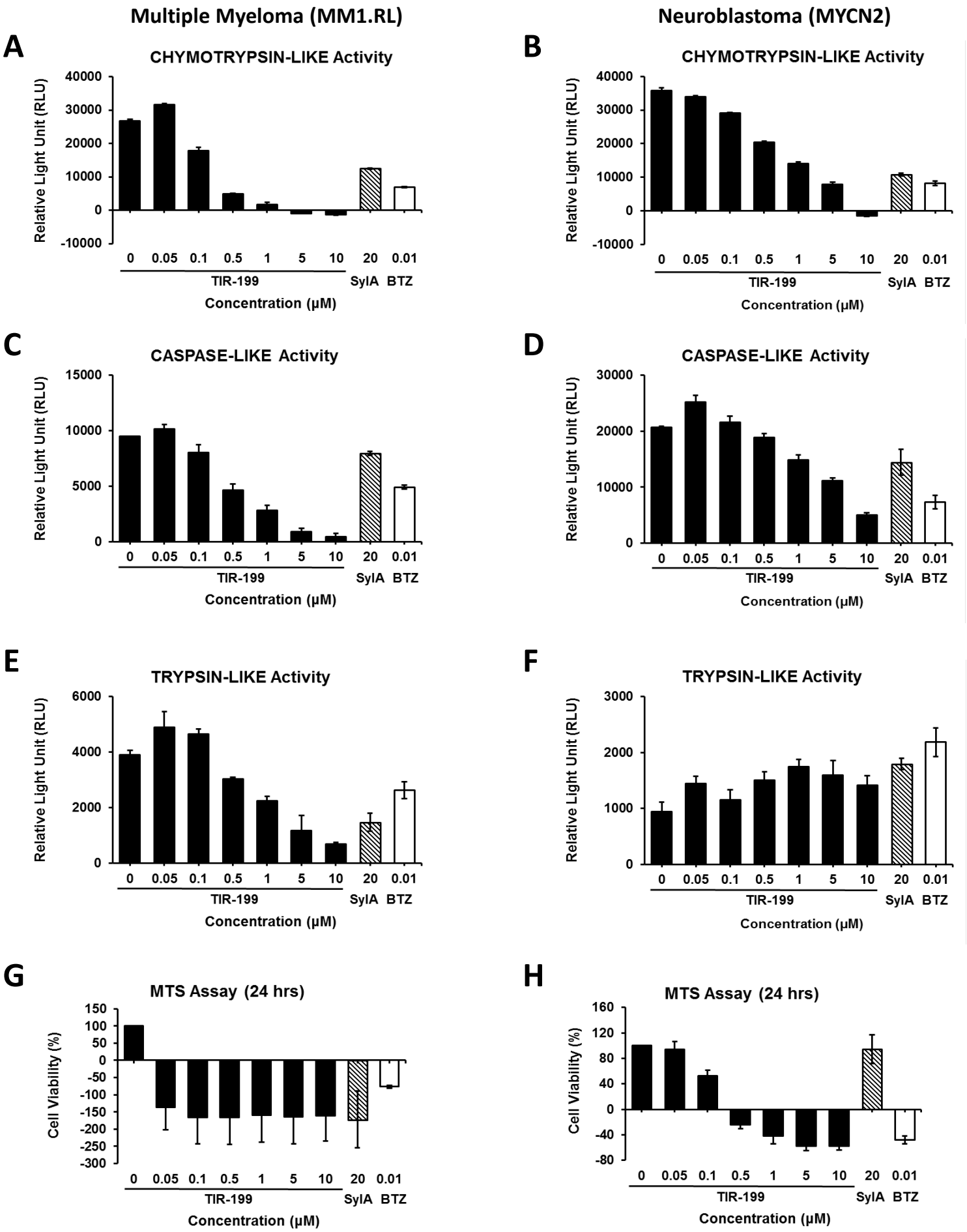
Multiple Myeloma (MM1.RL)
Neuroblastoma (MYCN2)
A
CHYMOTRYPSIN-LIKE Activity
B
CHYMOTRYPSIN-LIKE Activity
C
CASPASE-LIKE Activity
D
CASPASE-LIKE Activity
E
TRYPSIN-LIKE Activity
F
TRYPSIN-LIKE Activity
G
MTS Assay (24 hrs)
H
MTS Assay (24 hrs)
Relative Light Unit (RLU)
Cell Viability (%)
0 0.05 0.1 0.5 1 5 10 20 0.01
TIR-199
SylA BTZ
Concentration (μM)

Figure 5

A

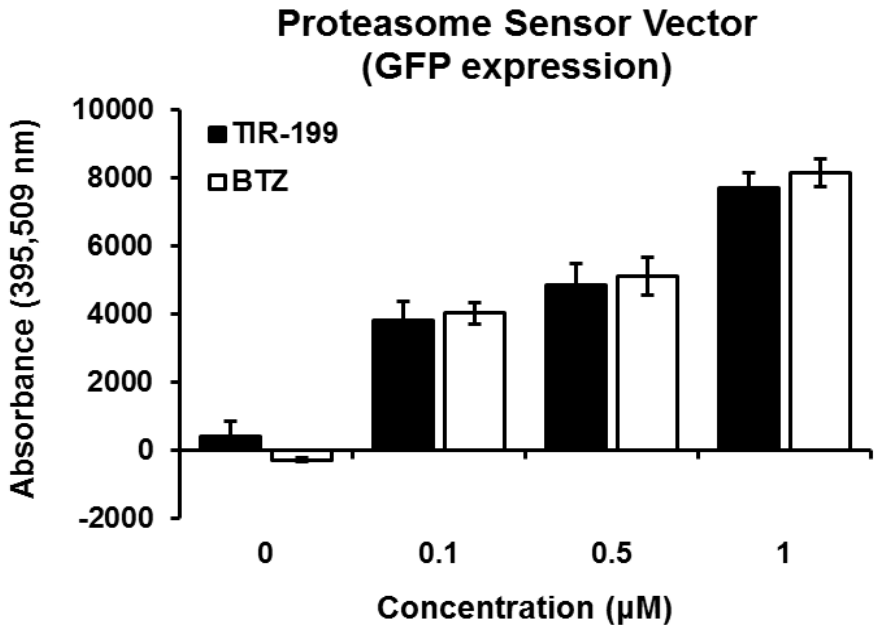
Proteasome Sensor Vector
(GFP expression)
Absorbance (395,509 nm)
10000
8000
6000
4000
2000
0
-2000
TIR-199
BTZ
0
0.1
0.5
1
Concentration (μM)

B

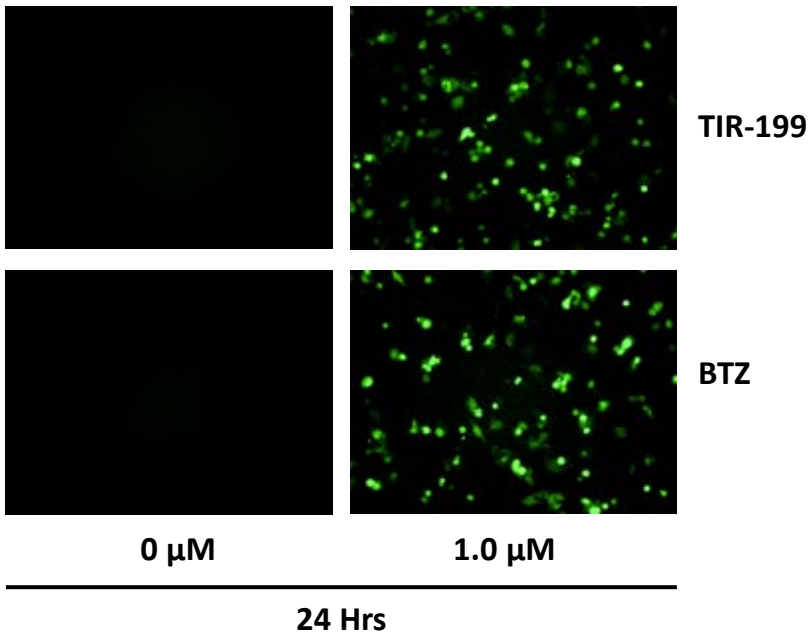
TIR-199
BTZ
0 μM
1.0 μM
24 Hrs

Figure 6

A

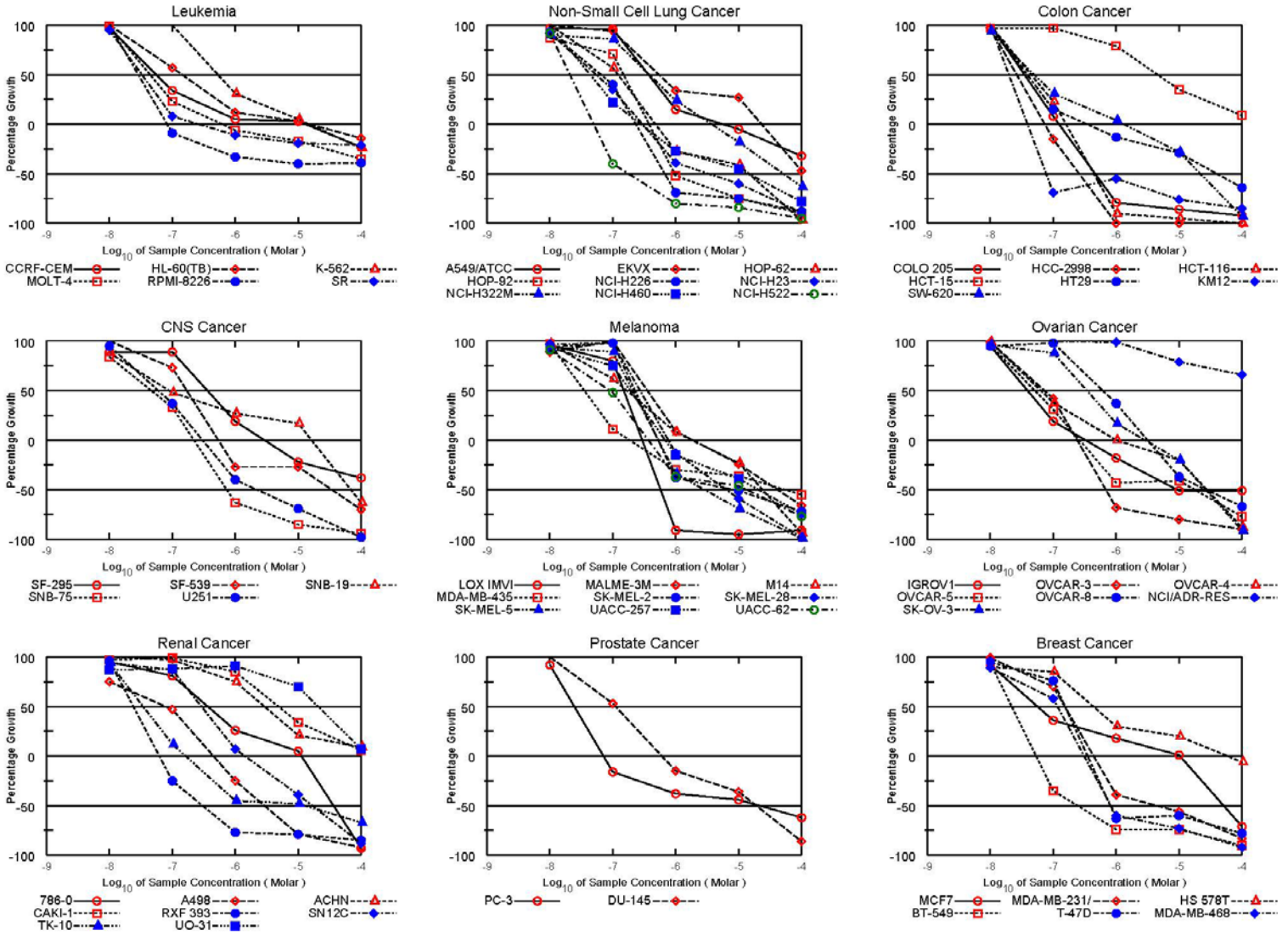

B

Panel Cell Line	Log_{10} GI50	GI50	Log_{10} TGI50	TGI	Log_{10} LC50	LC50
Leukemia						
CCRF-CEM	-7.25		-4.88		> -4.00	
HL-60(TB)	-6.85		-4.85		> -4.00	
K-562	-6.27		-4.84		> -4.00	
MOLT-4	-7.35		-6.19		> -4.00	
RPMI-8226	-7.54		-7.08		> -4.00	
SR	-7.48		-6.58		> -4.00	
Non-Small Cell Lung Cancer						
A549/ATCC	-6.43		-5.23		> -4.00	
EKVX	-6.26		-4.64		> -4.00	
HOP-62	-6.92		-6.32		-4.84	
HOP-92	-6.83		-6.42		-6.01	
NCI-H226	-7.19		-6.63		-6.18	
NCI-H23	-7.27		-6.53		-5.47	
NCI-H322M	-6.42		-5.43		-4.30	
NCI-H460	-7.35		-6.55		-4.86	
NCI-H522	-7.68		-7.30		-6.75	
Colon Cancer						
COLO 205	-7.45		-6.91		-6.33	
HCC-2998	-7.58		-7.13		-6.58	
HCT-116	-7.34		-6.80		-6.35	
HCT-15	-5.34		> -4.00		> -4.00	
HT29	-7.41		-6.46		-4.40	
KM12	-7.70		-7.40		-7.11	
SW-620	-7.30		-5.87		-4.66	
CNS Cancer						
SF-295	-6.45		-5.53		> -4.00	
SF-539	-6.77		-6.27		-4.46	
SNB-19	-7.04		-4.79		-4.16	
SNB-75	-7.34		-6.86		-6.13	
U251	-7.22		-6.52		-5.66	
Melanoma						
LOX IMVI	-6.83		-6.53		-6.24	
MALME-3M	-6.44		-5.73		-4.38	
M14	-6.77		-5.74		-4.62	
MDA-MB-435	-7.46		-6.74		-4.27	
SK-MEL-2	-6.65		-6.28		-5.10	
SK-MEL-28	-6.57		-6.11		-5.20	
SK-MEL-5	-6.68		-6.28		-5.55	
UACC-257	-6.72		-6.17		-4.68	
UACC-62	-7.05		-6.44		-4.88	
Ovarian Cancer						
IGROV1	-7.41		-6.49		-5.04	
OVCAR-3	-7.15		-6.62		-6.16	
OVCAR-4	-7.20		-5.99		-4.56	
OVCAR-5	-7.29		-6.58		-4.76	
OVCAR-8	-6.21		-5.50		-4.57	
NCI/ADR-RES	> -4.00		> -4.00		> -4.00	
SK-OV-3	-6.46		-5.55		-4.58	
Renal Cancer						
786-0	-6.43		-4.95		-4.44	
A498	-7.12		-6.35		-5.54	
ACHN	-5.53		> -4.00		> -4.00	
CAKI-1	-5.32		> -4.00		> -4.00	
RXF 393	-7.62		-7.21		-6.53	
SN12C	-6.54		-5.85		-4.77	
TK-10	-7.46		-6.78		-4.90	
UO-31	-4.68		> -4.00		> -4.00	
Prostate Cancer						
PC-3	-7.61		-7.15		-4.65	
DU-145	-6.96		-6.23		-4.72	
Breast Cancer						
MCF7	-7.25		-4.99		-4.29	
MDA-MB-231/ATCC	-6.82		-6.36		-5.34	
HS 578T	-6.37		-4.23		> -4.00	
BT-549	-7.66		-7.27		-6.62	
T-47D	-6.81		-6.45		-6.09	
MDA-MB-468	-6.94		-6.51		-6.09	
MID	-6.85		-5.98		-4.96	
Delta	0.85		1.42		2.15	
Range	3.7		3.4		3.11	

Figure 7

A

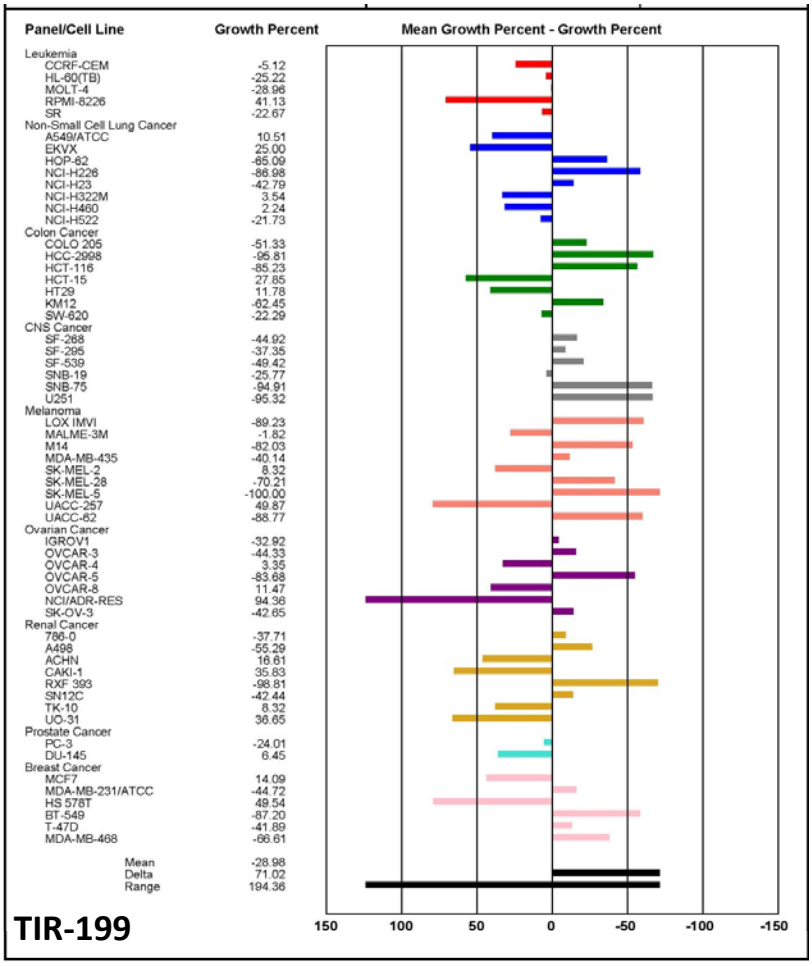
Panel/Cell Line
Growth Percent
Mean Growth Percent - Growth Percent
Leukemia
CCRF-CEM -5.12
HL-60(TB) -25.22
MOLT-4 -28.96
RPMI-8226 41.13
SR -22.67
Non-Small Cell Lung Cancer
A549/ATCC 10.51
EKVX 25.00
HOP-62 -65.09
NCI-H226 -86.98
NCI-H23 -42.79
NCI-H322M 3.54
NCI-H460 2.24
NCI-H522 -21.73
Colon Cancer
COLO 205 -51.33
HCC-2998 -95.81
HCT-116 -85.23
HCT-15 27.65
HT29 11.78
KM12 -62.45
SW-620 -22.29
CNS Cancer
SF-268 -44.92
SF-295 -37.35
SF-539 -49.42
SNB-19 -25.77
SNB-75 -94.91
U251 -95.32
Melanoma
LOX IMVI -89.23
MALME-3M -1.82
M14 -82.03
MDA-MB-435 -40.14
SK-MEL-2 8.32
SK-MEL-28 -70.21
SK-MEL-5 -100.00
UACC-257 49.87
UACC-62 -88.77
Ovarian Cancer
IGROV1 -32.92
OVCAR-3 -44.33
OVCAR-4 3.35
OVCAR-5 -83.68
OVCAR-8 11.47
NCI/ADR-RES 94.36
SK-OV-3 -42.65
Renal Cancer
786-0 -37.71
A498 -55.29
ACHN 16.61
CAKI-1 35.83
RXF 393 -98.81
SN12C -42.44
TK-10 8.32
UO-31 36.65
Prostate Cancer
PC-3 -24.01
DU-145 6.45
Breast Cancer
MCF7 14.09
MDA-MB-231/ATCC -44.72
HS 578T 49.54
BT-549 -87.20
T-47D -41.89
MDA-MB-468 -66.61
Mean -28.98
Delta 71.02
Range 194.36
150 100 50 0 -50 -100 -150
TIR-199

B

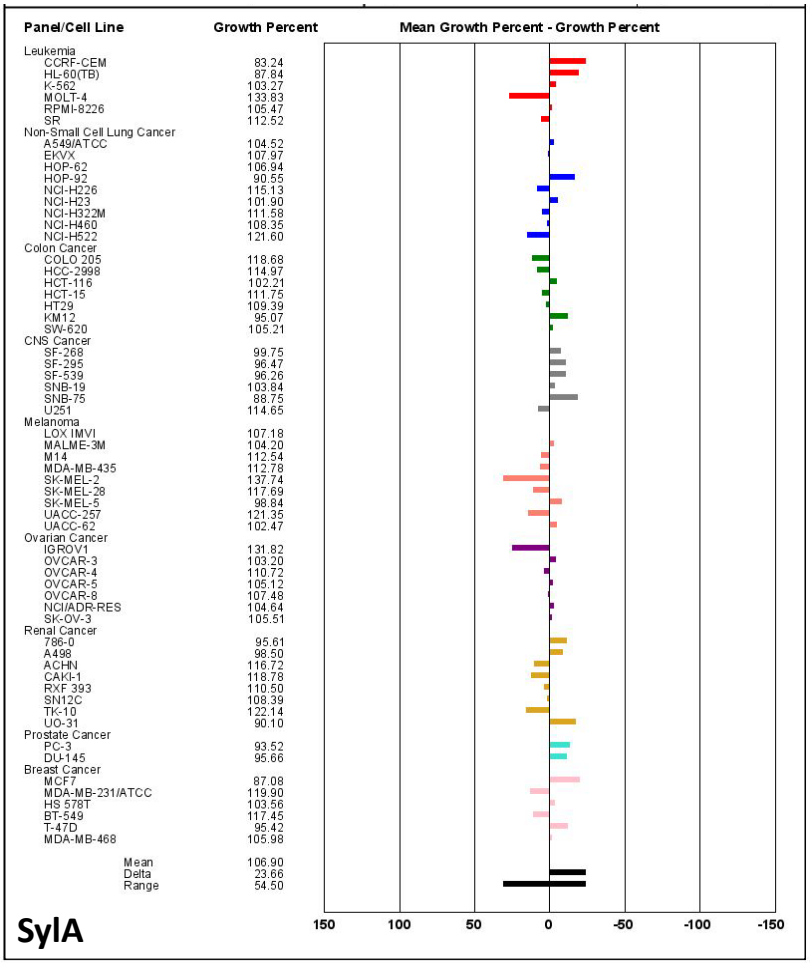
Panel/Cell Line
Growth Percent
Mean Growth Percent - Growth Percent
Leukemia
CCRF-CEM 83.24
HL-60(TB) 87.84
K-562 103.27
MOLT-4 133.83
RPMI-8226 105.47
SR 112.52
Non-Small Cell Lung Cancer
A549/ATCC 104.52
EKVX 107.97
HOP-62 106.94
HOP-92 90.55
NCI-H226 115.13
NCI-H23 101.90
NCI-H322M 111.58
NCI-H460 108.35
NCI-H522 121.60
Colon Cancer
COLO 205 118.68
HCC-2998 114.97
HCT-116 102.21
HCT-15 111.75
HT29 109.39
KM12 95.07
SW-620 105.21
CNS Cancer
SF-268 99.75
SF-295 96.47
SF-539 96.26
SNB-19 103.84
SNB-75 88.75
U251 114.65
Melanoma
LOX IMVI 107.18
MALME-3M 104.20
M14 112.54
MDA-MB-435 112.78
SK-MEL-2 137.74
SK-MEL-28 117.69
SK-MEL-5 98.84
UACC-257 121.35
UACC-62 102.47
Ovarian Cancer
IGROV1 131.82
OVCAR-3 103.20
OVCAR-4 110.72
OVCAR-5 105.12
OVCAR-8 107.48
NCI/ADR-RES 104.64
SK-OV-3 105.51
Renal Cancer
786-0 95.61
A498 98.50
ACHN 116.72
CAKI-1 118.78
RXF 393 110.50
SN12C 108.39
TK-10 122.14
UO-31 90.10
Prostate Cancer
PC-3 93.52
DU-145 95.66
Breast Cancer
MCF7 87.08
MDA-MB-231/ATCC 119.90
HS 578T 103.56
BT-549 117.45
T-47D 95.42
MDA-MB-468 105.98
Mean 106.90
Delta 23.66
Range 54.50
150 100 50 0 -50 -100 -150
SylA